

A Framework for Holistic KLD-based Waveform Design for Multi-User-Multi-Target ISAC Systems

Yousef Kloob, *Member, IEEE*, Mohammad Al-Jarrah, *Member, IEEE*, and Emad Alsusa, *Senior Member, IEEE*,

Abstract—This paper introduces a novel framework that leverages the Kullback-Leibler Divergence (KLD) metric to analyse and optimise performance trade-offs in integrated sensing and communication (ISAC) systems. We consider a multiple-input multiple-output (MIMO) base station that simultaneously serves communication user equipments (UEs) and detects multiple targets using a shared antenna deployment. We apply this framework to the widely used zero-forcing (ZF) communication beamforming technique, to assess their impact on the radar subsystem’s performance. Additionally, two optimisation problems are formulated: the first optimise the radar subsystem’s KLD under communication constraints, and the second focuses on communication waveform KLD optimisation with constraints on the radar KLD. These problems are solved using a projected gradient method with adaptive penalties for the radar waveforms and a gradient-assisted interior point method (IPM) for the communication waveforms. As performance benchmarks, we propose two additional optimisation frameworks: a radar waveform optimisation with bit error rate (BER) constraints and a communication waveform optimisation that minimises BER under radar KLD constraints. Theoretical derivations and simulations show that our KLD-based approach effectively characterises and optimises the ISAC performance trade-offs. Results indicate significant improvements in both radar detection and communication performance over conventional ZF beamforming and the identity covariance radar design, while achieving performance comparable to BER-based optimisation but with notably lower computational complexity. These findings highlight the advantages of KLD-based optimisation in balancing radar and communication performance for next-generation wireless networks.

Index Terms—Integrated sensing and communication, multiple-input-multiple-output (MIMO), radar, zero-forcing, beamforming, optimisation, Kullback-Leibler divergence (KLD).

I. INTRODUCTION

THE rapid evolution of wireless communication networks has dramatically expanded the landscape of interconnected devices to include new applications such as autonomous vehicles and unmanned aerial vehicles (UAVs) that are heavily dependent on advanced sensing, pushing the boundaries of communication systems beyond their traditional limits [1]–[4]. As we approach the sixth-generation (6G) era, network operators and service providers aim not only to further enhance their communication services but also to include advanced sensing-based applications such as detection, localisation, tracking, navigation, and environmental surveillance [5]–[7].

Integrated Sensing and Communications (ISAC) systems have gained significant interest as a key enabler of many 6G applications. ISAC aims to synergistically merge sensing and communication functionalities hence optimising base station (BS)

Y. Kloob, M. Al-Jarrah and E. Alsusa are with the Department of Electrical and Electronic Engineering, University of Manchester, Manchester M13 9PL, U.K. (e-mail: {yousef.kloob, mohammad.al-jarrah, e.alsusa}@manchester.ac.uk).

resources for dual purposes [8]–[13]. This integration can be achieved through various approaches. For example, in a separated deployment, the BS antennas are allocated distinctly between communication and radar subsystems, which can simplify the system design but may underutilise resources. In contrast, the shared deployment strategy employs all antennas for both functionalities, hence offering higher resource efficiency, but at the cost of increased complexity due to the need for more sophisticated signal processing techniques [14], [15].

The evolution of ISAC has been accelerated by advances in multi-antenna technologies, particularly massive Multiple-Input Multiple-Output (MIMO) systems, which significantly enhance both communication capacity and sensing accuracy [16]. However, evaluating the performance of ISAC systems poses unique challenges due to their dual functionality. Traditionally, communication and sensing subsystems have been assessed using distinct metrics—communication performance through achievable rate, outage probability, and bit error rate (BER), and sensing performance through estimation rate, detection probability, false alarm probability, and mean square error (MSE) [17]. This disparity complicates the holistic assessment and optimisation of ISAC systems.

A. Literature review

To address these challenges mentioned above, there has been a growing interest in developing unified design tools that can simultaneously capture both sensing and communication capabilities. One such tool that has gained traction is the Kullback-Leibler divergence (KLD), also known as the relative entropy. KLD has a well-established history in information theory and has been extensively used in the analysis and design of sensing systems, particularly in the context of MIMO radars [18]–[20]. It quantifies the dissimilarity between two probability distributions, serving as a measure of the information gain achieved by using one distribution over another. While the application of KLD in sensing systems is well-established, its potential in characterising communication system performance remains open. Recent studies have begun to bridge this gap, demonstrating the utility of KLD in assessing the performance trade-offs between sensing and communication functionalities in ISAC systems. For instance, in our previous works [21], [22], we employed KLD to analyse the performance trade-off in ISAC systems with separated antenna deployment, relating radar detection probability P_D and communication BER to the achievable KLD. This stems from the fact that KLD is intrinsically tied to maximum-likelihood detection, long used in radar and equally central to communication receivers, whose errors are quantified by BER. Consequently, KLD can quantify the detection capability at both the radar and communication ends in a similar manner, making it a powerful, unified design tool for ISAC systems. While in [23] we proposed a low-complexity unified objective function based on KLD, the aim was focused on optimising network resources for both separated and shared deployment scenarios. Moreover, further insights about the

achievable KLD trade-off in ISAC systems are explored in [24], and more useful designs have been discovered. Nonetheless, the literature lacks a comprehensive investigation and beamforming design for a generalised multi-user-multi-target (MUMT) ISAC system using the promising KLD.

Further efforts have explored various optimisation approaches for ISAC systems, each addressing specific aspects of system performance. For example, joint radar-communication beamforming optimisation based on the Cramér-Rao Bound (CRB) has been proposed to improve both sensing and communication performance [25], where this approach minimises the CRB of angle estimation while maximising the signal-to-interference-plus-noise ratio (SINR) for communication. However, these methods often focus on optimising individual components rather than adopting a unified framework that captures the interplay between different functionalities. Beamforming optimisation has been a particular focus, with studies investigating partially connected hybrid designs to address hardware complexity issues [26]. While these approaches offer some practical advantages in terms of implementation, they fail to fully capture the nuanced trade-offs between sensing and communication performance in deeply integrated scenarios. Similarly, waveform optimisation has also been extensively studied, with recent work using faster-than-Nyquist approaches to enhance spectral efficiency while maintaining radar functionality as a constraint [27]. Despite these advances, existing work has not adequately addressed the need for a unified optimisation framework that simultaneously serves both subsystems' requirements and balances their performance trade-offs effectively.

B. Motivation and contribution

Despite these advances, current approaches often fall short of fully exploiting the potential of integrated systems. Most notably, there is a need for more comprehensive models that accurately reflect the real-world operation of ISAC systems, particularly in scenarios where communication signals can be utilised for radar target detection alongside dedicated radar signals. Exploiting the interference from communication signals as a source of information for radar operations enhances radar detection capabilities, improving the system's overall resource efficiency [14]. This dual-use of communication signals represents a significant departure from traditional approaches, which typically treat interference as a detrimental factor to be mitigated rather than leveraged [28], [29].

Toward these objectives and motivated by the fact that KLD is able to provide a unified measure for ISAC systems holistically, this paper proposes a novel framework based on the KLD as a design tool to optimise the sensing-communication performance trade-offs in shared antenna deployment based ISAC systems. This work addresses significant issues in the existing literature by introducing a unified KLD-based waveform design that captures the synergies and trade-offs between sensing and communication in ISAC systems, through well-established relations between KLD from one side, and the detection probability in radar via Stein's Lemma and BER in communication systems from the other side [21]. By considering the shared deployment scenario and proposing specific optimisation techniques for both subsystem waveforms, we provide a comprehensive approach for system optimisation that reflects the true potential of ISAC systems in future wireless networks. Our system model consists of a MIMO

BS that simultaneously serves communication user equipment (UEs) and detects multiple targets using shared resources. The key contributions of this work are:

- **Unified Design Tool:** We derive the KLD specifically for the integrated operation of communication and radar systems in ISAC. The established KLD consolidates the communication error rate and radar target detection capabilities into a single objective function while offering enhanced analytical tractability compared to traditional performance metrics (e.g., BER), our approach enables a holistic system optimisation that synergistically improves overall performance.
- **Exploitation of Communication Interference:** Our framework accounts for the fact that communication signals can also be exploited for radar target detection alongside dedicated radar signals, providing a more comprehensive and useful model of ISAC system operation. This dual-use approach enhances the radar performance by utilising communication interference as an additional source of information for target detection.
- **KLD-based Optimised ISAC:** We propose two novel optimisation techniques: radar and communication waveform KLD-based optimisation. Both maximise their respective KLD measures subject to the minimum KLD of both subsystems and power constraints. The non-convex radar optimisation employs a projected gradient method with an adaptive penalty, while the communication optimisation uses a gradient-assisted interior point method. These techniques efficiently handle ISAC waveform design's complex nature, enabling balanced performance optimisation across both subsystems within system constraints.
- **Benchmark Analysis:** We compare the proposed KLD-based strategies against the conventional zero-forcing (ZF) beamforming for the communication subsystem and the identity covariance design for the radar subsystem. In addition, we introduce two optimisation frameworks based on the BER to further benchmark our methods. These comparisons highlight the performance gains, computational trade-offs, and practical relevance of our KLD-based approach in a range of ISAC scenarios.

Our results demonstrate that the proposed KLD-based optimisation techniques significantly outperform ZF beamforming and the radar subsystem's identity covariance baseline, as well as the BER-based designs in terms of computational cost. The radar waveform optimisation shows substantial improvements in both target detection and communication performance, while the communication waveform optimisation primarily benefits the communication subsystem with modest radar performance gains. Both techniques exhibit robust performance across varying SNR levels, with the radar optimisation demonstrating particularly stable computational efficiency. Beyond its direct links to conventional performance metrics, KLD also facilitates a more structured and scalable optimisation framework—unlike complex BER-based designs, KLD-based formulations as evidenced by our numerical results offer more computational efficiency. Notably, utilising the communication signals in radar detection significantly enhances overall system performance, especially in scenarios with limited dedicated radar resources. These highlight the practical significance of KLD-based waveform design and provide valuable insights for developing efficient shared deployment ISAC systems that balance sensing and communication requirements.

C. Paper organisation

The paper is structured as follows. Section II presents the system model. Sections III and IV analyse the communication and radar systems, respectively, including the derivations of KLD for each system. In Section V, the radar waveform is optimised considering two approaches KLD-based and a BER constrained both are investigated. Section VI, the communication waveform is optimised considering two approaches KLD-based and BER-based both are investigated. Section VII shows the complexity analysis for the waveform optimisation techniques, Section VIII displays the numerical results, and finally, Section IX concludes the work.

Notation: Bold uppercase letters (e.g., \mathbf{S}) denote matrices, and bold lowercase letters (e.g., \mathbf{s}) denote vectors. Superscripts $(\cdot)^*$, $(\cdot)^T$, and $(\cdot)^H$, denote the conjugate, transpose, and Hermitian transpose, respectively. Subscripts $(\cdot)_c$ and $(\cdot)_r$ relate to the communication, and radar subsystems, respectively.

II. SYSTEM MODEL

We consider an N antenna MIMO-BS. The antennas are utilised for detecting a maximum number of T targets and serving K number of single-antenna communication UEs in the downlink direction in shared deployment manner. The total transmitted power available at BS is P_T which is utilised for both sensing and data communication duties. The power P_T allocated to the radar and communication subsystems are denoted as P_r and P_c , where $P_T = P_c + P_r$. As a starting point, non-optimised ZF beamforming technique is employed at BS to precode the information of communication UEs [16]. These techniques serve as benchmarks for our subsequent optimised systems, which will be introduced and analysed later in Sections V and VI. The combined transmitted ISAC signal $\mathbf{x}_l \in \mathbb{C}^{N \times 1}$ at the l -th snapshot can be formulated as follows,

$$\mathbf{x}_l = \mathbf{W}_c \mathbf{s}_{c,l} + \mathbf{W}_r \mathbf{s}_r, \quad (1)$$

where $l \in \{1, 2, \dots, L\}$ represents the discrete time index, and L is the total number of snapshots considered for sensing outcome, $\mathbf{s}_{c,l} \in \mathbb{C}^{K \times 1}$ is a vector of communication UEs symbols, $\mathbf{s}_r \in \mathbb{C}^{T \times 1}$ is a vector of the baseband radar waveforms for the potential targets, $\mathbf{W}_c \in \mathbb{C}^{N \times K}$ represents the precoding matrix for the communication subsystem, and $\mathbf{W}_r \in \mathbb{C}^{N \times T}$ represents the precoding matrix for the radar subsystem. The transmitted signals vector \mathbf{x}_l is transmitted from the BS and received at the UEs as well as the targets which reflect the received \mathbf{x}_l back to the BS. Although the radar signal component received at the UEs might cause interference that cannot be eliminated by the users, the communication signal component received at the targets and reflected back to the BS carries information about the target. Therefore, by carefully designing the precoding matrices at the BS, the sensing information can be enhanced by exploiting the communication signal. This dual-use approach enhances the radar performance by utilising the communication signal as an additional source of information. The radar waveform design is based on the combined transmit signal covariance matrix for the t -th beam where the covariance matrix of the t -th transmit beam is $\mathbf{R}_t = \frac{1}{L} \sum_{l=1}^L \mathbf{x}_{t,l} \mathbf{x}_{t,l}^H$, $\mathbf{x}_{t,l} = \mathbf{w}_{r,t,l} s_{r,t} + \mathbf{W}_c \mathbf{s}_{c,l}$. This formulation allows us to incorporate the communication signals into the radar detection process. It should be noticed that the power for the radar is integrated into the precoding vector $\mathbf{w}_{r,t,l}$, where it is designed to have $\|\mathbf{w}_{r,t,l}\|_F^2 = \frac{P_r}{T}$, and $\mathbf{w}_{r,t,l} = \frac{P_r}{NT} \tilde{\mathbf{w}}_{r,t,l}$, where

$\tilde{\mathbf{w}}_{r,t,l}$ is the t th beam precoding vector, and $\|\cdot\|_F$ is the Frobenius norm.

A. Communication System

At each l instance, a data symbol $s_{c,k,l}$ intended for the k -th UE is drawn from a normalised constellation, i.e, $\mathbb{E}[|s_{c,k,l}|^2] = 1$. The received signal at the k -th UE can be formulated as

$$y_{c,k,l} = \underbrace{\mathbf{h}_k^T d_{c,k}^{-\zeta/2} \mathbf{w}_{c,k} s_{c,k,l}}_{\text{Desired } k\text{-th UE signal}} + \underbrace{\omega_{MN,k}}_{\text{Inter-user interference}} + \underbrace{\eta_k}_{\text{Radar interference and noise}}, \quad (2)$$

where $\mathbf{h}_k \in \mathbb{C}^{N \times 1} \sim \mathcal{CN}(0, \sigma_h^2)$ represents the channel from the BS to the k -th UE, $\omega_{MN,k} = \sum_{i=1, i \neq k}^K \mathbf{h}_k^T d_{c,k}^{-\zeta/2} \mathbf{w}_{c,i} s_{c,i,l}$ represents the IUI on the k -th UE from the other UEs, $d_{c,k}^{-\zeta/2}$ is the channel pathloss from BS to the k -th UE with $d_{c,k}$ representing the distance from BS to the k -th UE, and ζ is the pathloss exponent $\eta_k = \mathbf{h}_k^T d_{c,k}^{-\zeta/2} \mathbf{W}_{r,l} \mathbf{s}_{r,l} + n_{k,l}$ is the interference-plus-noise term with $n_{k,l} \sim \mathcal{CN}(0, \sigma_n^2)$ representing the additive white Gaussian noise (AWGN). The precoding vector for the communication system is $\mathbf{w}_{c,k} \in \mathbb{C}^{N \times 1}$, which is typically designed based on the given channel matrix from MIMO-BS to UEs $\mathbf{H} \in \mathbb{C}^{N \times K} = [\mathbf{h}_1, \dots, \mathbf{h}_k, \dots, \mathbf{h}_K]$, where the elements of \mathbf{H} are independent and identically distributed (i.i.d) complex Gaussian random variables with zero mean and variance σ_h^2 . ZF designs which is typically used to precode the communication data symbols at the BS. This precoding scheme will serve as a benchmark for our designs. The ZF precoding eliminates inter-user interference (IUI) at the UEs regardless of the amount of the received power. This approach usually results in excellent performance at high SNR values. The normalised ZF beamforming matrix is designed also based on the channel matrix, and can be represented as follows,

$$\mathbf{W}_c = \mathbf{P} \tilde{\mathbf{W}}_c / \|\tilde{\mathbf{W}}_c\|_F \quad (3)$$

where $\tilde{\mathbf{W}}_c = \mathbf{H}^H (\mathbf{H} \mathbf{H}^H)^{-1}$ is the ZF beamformer before normalisation, and $\mathbf{P} \in \mathbb{C}^{K \times K} = \text{diag}(\sqrt{p_1}, \dots, \sqrt{p_K})$ is the power allocation matrix for the communication users, which is a diagonal matrix that controls the power allocated for each UE.

B. Radar system

The radar system is designed for high adaptability, allowing for real-time adjustments in detection capabilities across L frame snapshots. T represents the radar beams emitted during a specific detection frame. Using MIMO radar technology, multiple beams can be generated simultaneously using orthogonal signals [30], [31], where T signifies the upper limit of detectable targets in a single frame.

The system explores multiple angular-range-Doppler bins over successive frames, increasing target identification. Its flexibility in varying emitted beams allows for the simultaneous detection of more targets, to fine-tune the system's detection capability according to different operational demands. However, it is crucial to acknowledge that the value of T is constrained by the available antennas and UEs serviced by the BS, highlighting the need for efficient waveform design and resource allocation in ISAC systems. Our focus aligns with scenarios where targets are spatially separated, with each target confined to a distinct radar bin, as per prior studies [32], [33]¹. The total radar return signal at the l -th snapshot is shown as follows,

¹The literature presents algorithms to separate signals from closely spaced or unresolved targets, facilitating accurate target enumeration [34].

$$\mathbf{y}_{r,l} = \sum_{t=1}^T \mathbf{H}_t^T d_{r,t}^{\zeta/2} \mathbf{w}_{r,t,l} s_{r,t} + \mathbf{H}_t^T d_{r,t}^{\zeta/2} \mathbf{W}_c \mathbf{s}_{c,l} + \mathbf{n}_l, \quad (4)$$

where $\mathbf{H}_t \in \mathbb{C}^{N \times N}$ is the target response matrix that captures the complete BS-Target-BS path characteristics for the t -th target, inherently incorporating propagation effects, target cross-section, and reflection coefficients. The target response matrix follows a Rayleigh distribution to model the composite effects of multiple scattering centres inherent in extended targets, thereby characterising the statistical nature of target scattering while preserving the direct path essential for target detection [35], [36]. The $\mathbf{n}_l \sim \mathcal{CN}(\mathbf{0}, \sigma_n^2 \mathbf{I}_N)$ is the AWGN vector at the l -th snapshot. To process the radar returns from all beams, a bank of matched filters is typically applied, each tuned to a specific waveform $s_{r,t} : \forall t = \{1, 2, \dots, T\}$, which corresponds to a particular radar angular-range-Doppler bin. Assuming $s_{r,t}$ is orthogonal to $s_{r,i}$ for all $t \neq i$ using signal space and time domain, the radar returns from distinct beams can be effectively separated, enabling independent detection of each potential target [31], [36]. The radar precoding matrix $\mathbf{W}_{r,l}$ is designed such that the covariance matrix is $\mathbf{R}_w \triangleq \frac{1}{L} \sum_{l=1}^L \mathbf{W}_{r,l} \mathbf{W}_{r,l}^H \in \mathbb{C}^{N \times N}$. The received signal for the t -th target at the BS after match-filtering, under the binary hypothesis testing problem $\mathcal{H}_q \forall q \in \{0, 1\}$, where \mathcal{H}_1 represents the target presence whereas \mathcal{H}_0 denotes the target absence, is denoted by $\mathbf{y}_{r,t,l|\mathcal{H}_q}$ and can be mathematically represented as follows,

$$\mathbf{y}_{r,t,l|\mathcal{H}_q} = \mathbf{H}_t^T d_{r,t}^{\zeta/2} \mathbf{w}_{r,t,l} q + \mathbf{H}_t^T d_{r,t}^{\zeta/2} \mathbf{W}_c \mathbf{s}_{c,l} q + \mathbf{n}_{t,l}, \quad (5)$$

where $\mathbf{n}_{t,l} \sim \mathcal{CN}(\mathbf{0}, \sigma_n^2 \mathbf{I}_N)$ is the AWGN vector at the l -th snapshot at the output of the matched filter.

III. THE COMMUNICATION KLD: ZF AND ARBITRARY PRECODING MATRIX

In this section, we derive the KLD of the communication system for ZF beamforming with shared deployment antenna configuration, where the KLD quantifies the distinguishability between different transmitted symbols by measuring the information divergence of their received signal distributions, capturing the fundamental ability to differentiate communication symbols at the receiver. The analysis is carried out for the normalised precoders introduced in Section II-A. To derive the KLD, it is necessary to establish the statistical properties of the signal, IUI, radar interference, and noise. For a pair of multivariate Gaussian distributed random variables having mean vectors of μ_m and μ_n and covariance matrices of Σ_m and Σ_n , the KLD can be derived as,

$$\text{KLD}_{n \rightarrow m} = \frac{1}{2 \ln 2} \left(\text{tr}(\Sigma_n^{-1} \Sigma_m) - 2 + (\mu_n - \mu_m)^T \times \Sigma_n^{-1} (\mu_n - \mu_m) + \ln \frac{|\Sigma_n|}{|\Sigma_m|} \right). \quad (6)$$

A. ZF beamforming

With ZF precoding, the received signal at the k -th user is,

$$y_{k,l} = \mathbf{h}_k^T d_{c,k}^{-\zeta/2} \mathbf{w}_{c,k} s_{c,k} + \mathbf{h}_k^T d_{c,k}^{-\zeta/2} \mathbf{W}_c \mathbf{s}_{c,l} + n_{k,l}, \quad (7)$$

where $\mathbf{w}_{c,k}$ is the k -th column of the normalised ZF precoding matrix. Note, that the term $\sum_{i=1, i \neq k}^K \mathbf{h}_k^T d_{c,k}^{-\zeta/2} \mathbf{w}_{c,i} s_{c,i,l} = 0$ as the ZF precoder eliminates the IUI. The distribution of η_k is well approximated by a complex Gaussian distribution using

CLT, particularly for large N . This approximation yields a mean of $\mathbb{E}[\eta_k] = 0$, and a variance of,

$$\sigma_\eta^2 = d_{c,k}^{-\zeta} \mathbb{E}[\|\mathbf{h}_k^T \mathbf{W}_{r,l}\|^2] + \sigma_n^2 = d_{c,k}^{-\zeta} P_r \sigma_h^2 + \sigma_n^2 \quad (8)$$

where $\mathbf{R}_{w,t} = \frac{1}{L} \sum_{l=1}^L \tilde{\mathbf{w}}_{r,t,l} \tilde{\mathbf{w}}_{r,t,l}^H$. The mean vectors and covariance matrices for the n -th and m -th symbols are given by,

$$\begin{aligned} \mu_{k,j} &= d_{c,k}^{-\zeta/2} \mathbb{E}[\mathbf{h}_k^T \mathbf{w}_{c,k}] s_{c,k,l}^{(j)} \\ &= d_{c,k}^{-\zeta/2} \mathbb{E}[\|\tilde{\mathbf{W}}_c\|_F^{-2}] s_{c,k,l}^{(j)}, \quad j \in \{n, m\}, \end{aligned} \quad (9)$$

$$\Sigma_n = \Sigma_m = \sigma_\eta^2, \quad (10)$$

where $\mathbb{E}[\mathbf{h}_k^T \mathbf{w}_{c,k}] = 1$ due to the normalisation of the ZF precoding matrix. Since $\|\tilde{\mathbf{W}}_c\|_F^{-2} = \text{tr}((\mathbf{H}\mathbf{H}^H)^{-1})$, under flat fading channel, $\|\tilde{\mathbf{W}}_c\|_F^{-2}$ follows a Gamma distribution with shape parameter $N - K + 1$ and scale parameter 1, denoted as $\|\tilde{\mathbf{W}}_c\|_F^{-2} \sim \text{Gamma}(L_G, 1)$, where $L_G = N - K + 1$. Let $x \triangleq \|\tilde{\mathbf{W}}_c\|_F^2$. By substituting (9), and (10) in (6), and considering all possible pairs of dissimilar symbols [21, Corollary 1], then the KLD becomes,

$$\text{KLD}_{c,k}^{\text{ZF}} = \frac{\lambda d_{c,k}^{-\zeta} p_k}{M(M-1)\sigma_\eta^2 \ln 2} \mathbb{E} \left[\frac{1}{\|\tilde{\mathbf{W}}_c\|_F^2} \right], \quad (11)$$

where $\lambda = \sum_{m=1}^M \sum_{\substack{n=1 \\ n \neq m}}^M \left| s_{c,k,l}^{(n)} - s_{c,k,l}^{(m)} \right|^2$ is a constant that depends on the constellation. The expectation of $1/\|\tilde{\mathbf{W}}_c\|_F^2$ can be calculated using the PDF of Gamma distribution as follows,

$$\mathbb{E}[\|\tilde{\mathbf{W}}_c\|_F^{-2}] = \int_0^\infty \frac{1}{x} \cdot \frac{1}{\Gamma(L_G)} x^{L_G-1} e^{-x} dx = N - K. \quad (12)$$

Substituting this result into (11), we get the final $\text{KLD}_{c,k}^{\text{ZF}}$,

$$\text{KLD}_{c,k}^{\text{ZF}} = \lambda d_{c,k}^{-\zeta} p_k (N - K) / M(M-1)\sigma_\eta^2 \ln 2. \quad (13)$$

B. Conditional KLD for an Arbitrary Precoding Matrix \mathbf{W}_c and Given Channel Matrix

A conditional KLD for communication, in terms of the beamforming matrix \mathbf{W}_c and for a given channel matrix \mathbf{H} , is required to formulate an optimisation problem. Considering the received signal representation in (2), the conditional mean vectors and variance are,

$$\mu_{k,j} = \mathbb{E}[y_{c,k,l}^{(j)}] = \mathbf{h}_k^T d_{c,k}^{-\zeta/2} \mathbf{w}_{c,k} s_{c,k,l}^{(j)}, \quad j \in \{n, m\}, \quad (14)$$

$$\begin{aligned} \text{Var}(y_{c,k,l}^{(j)}) &= \mathbb{E}[|y_{c,k,l}^{(j)} - \mu_{k,n}|^2] \\ &= d_{c,k}^{-\zeta} \sum_{i=1, i \neq k}^K \|\mathbf{h}_k^T \mathbf{w}_{c,i}\|^2 + \sigma_\eta^2, \quad j \in \{n, m\}, \end{aligned} \quad (15)$$

Note that, the variance of the received signal for a given pair of symbols $\{s_{c,k,l}^{(n)}, s_{c,k,l}^{(m)}\} \forall \{m, n\}, m \neq n$ is equal. Thus, the covariance is,

$$\Sigma_{c,n} = \Sigma_{c,m} = d_{c,k}^{-\zeta} \sum_{i=1, i \neq k}^K \|\mathbf{h}_k^T \mathbf{w}_{c,i}\|^2 + \sigma_\eta^2, \quad (16)$$

by substituting the evaluated mean vectors and covariance matrices in (14), and (16) into the KLD expression given in (6), we can obtain the KLD for the k -th UE in the communication subsystem for each possible pair of unequal data symbols $\{s_{c,k,l}^{(n)}, s_{c,k,l}^{(m)}\}, n \neq m$, which can be represented as follows,

$$\text{KLD}_{c,k}^{m \rightarrow n} = \frac{d_{c,k}^{-\zeta}}{2 \ln 2} \left(\left(\mathbf{h}_k^T \mathbf{w}_{c,k} (s_{c,k,l}^{(m)} - s_{c,k,l}^{(n)}) \right)^H \right. \\ \left. \times \left(d_{c,k}^{-\zeta} \sum_{i=1, i \neq k}^K \|\mathbf{h}_k^T \mathbf{w}_{c,i}\|^2 + \sigma_\eta^2 \right)^{-1} \left(\mathbf{h}_k^T \mathbf{w}_{c,k} (s_{c,k,l}^{(m)} - s_{c,k,l}^{(n)}) \right) \right). \quad (17)$$

Thereafter, by considering all possible pairs of dissimilar symbols, then the KLD expression using λ is simplified as,

$$\text{KLD}_{c,k}^{m \rightarrow n} = \frac{\lambda d_{c,k}^{-\zeta}}{2M(M-1) \ln 2} \times \frac{\|\mathbf{h}_k^T \mathbf{w}_{c,k}\|^2}{d_{c,k}^{-\zeta} \sum_{i=1, i \neq k}^K \|\mathbf{h}_k^T \mathbf{w}_{c,i}\|^2 + \sigma_\eta^2}. \quad (18)$$

It should be noted that the second term in this equation, represents a form of the SINR, where the interference is the sum of IUI and radar interference.

IV. RADAR SYSTEM ANALYSIS

A. Composite detection and response matrix estimation

The main objective of typical radar systems is to detect the existence of targets and estimate the matrix response for existing targets. After separating signals associated with different targets, we formulate a composite detection-estimation problem as follows,

$$\{\hat{\mathbf{H}}_t, \mathcal{H}_q\} = \arg \max_{\mathbf{H}_t, \mathcal{H}_q \forall q \in \{0,1\}} f(\mathbf{y}_{r,t,l}; \mathbf{H}_t, \mathbf{x}_{t,l}, \mathcal{H}_q). \quad (19)$$

This joint optimisation problem aims to simultaneously detect the presence of a target, i.e., determining $\hat{\mathcal{H}}_q$, and estimate its response matrix $\hat{\mathbf{H}}_t$ if presents. It can be observed from (5) that the distribution of the received signals vector $\mathbf{y}_{r,t,l}$ under each hypothesis is multivariate normal whose PDF is,

$$f(\mathbf{y}_{r,t,l}; \mathbf{H}_t q, \mathbf{x}_{t,l} q, \mathcal{H}_q) = \frac{1}{\pi^N [(1-q)\sigma_n^{2N} + q \det(\mathbf{R}_{1,t})]} \\ \times \exp \left(-\mathbf{y}_{r,t,l}^H [(1-q)\sigma_n^{-2} + q \det(\mathbf{R}_{1,t})] \mathbf{y}_{r,t,l} \right), \quad (20)$$

where $\mathbf{R}_{1,t} = \mathbf{H}_t \mathbf{R}_{t,l} \mathbf{H}_t^H + \sigma_n^2 \mathbf{I}_N$, and $\mathbf{R}_{t,l} = \mathbf{x}_{t,l} \mathbf{x}_{t,l}^H d_{r,t}^\zeta$. The generalised likelihood ratio test (GLRT) for the t -th target is used to determine target existence or absence by comparing the likelihoods under the two hypotheses, which is derived as,

$$\Lambda_{t,l} = \frac{\arg \max_{\mathbf{H}_t} f(\mathbf{y}_{r,t,l}; \mathbf{H}_t, \mathbf{x}_{t,l}, \mathcal{H}_1)}{\arg \max_{\mathbf{H}_t} f(\mathbf{y}_{r,t,l}; \mathcal{H}_0)}. \quad (21)$$

As the PDF does not depend on \mathbf{H}_t under \mathcal{H}_0 , the target response matrix is estimated under \mathcal{H}_1 , thus by using the maximum likelihood estimation theorem, we obtain,

$$\hat{\mathbf{H}}_t = \arg \max_{\mathbf{H}_t} f(\mathbf{y}_{r,t,l}; \mathbf{H}_t, \mathbf{x}_{t,l}, \mathcal{H}_1). \quad (22)$$

Since the PDF of $\mathbf{y}_{r,t,l}$ is multivariate Gaussian, the maximisation leads to the least squares solution given by,

$$\hat{\mathbf{H}}_t = \arg \min_{\mathbf{H}_t} \|\mathbf{y}_{r,t} - \mathbf{H}_t \mathbf{x}_{t,l}\|^2 = \mathbf{y}_{r,t} \mathbf{x}_{t,l}^H (\mathbf{x}_{t,l} \mathbf{x}_{t,l}^H)^{-1}. \quad (23)$$

This least squares solution provides an unbiased estimate of the target-response matrix \mathbf{H}_t , with accuracy directly tied to the detection probability P_D . When the radar correctly detects a target under \mathcal{H}_1 , the maximum likelihood solution $\hat{\mathbf{H}}_t$ is used to estimate \mathbf{H}_t . In contrast, a miss detection (i.e., deciding \mathcal{H}_0 under \mathcal{H}_1) forces $\hat{\mathbf{H}}_t = \mathbf{0}$, resulting in significant errors. The overall unconditional MSE is defined as,

$$\text{MSE} = p(H_1) \left[(1 - P_D) \text{MSE}_{0,1} + P_D \text{MSE}_{1,1} \right] \\ + [1 - p(H_1)] \left[P_{\text{FA}} \text{MSE}_{1,0} \right], \quad (24)$$

where $p(H_1)$ is the prior probability of target existence with equal probability assumed, $\text{MSE}_{1,1} \triangleq \mathbb{E}[\|\hat{\mathbf{H}}_t - \mathbf{H}_t\|^2 | \mathcal{H}_q = \mathcal{H}_1, \hat{\mathcal{H}}_q = \mathcal{H}_1]$ is the MSE under correct detection, $\text{MSE}_{1,0} \triangleq \mathbb{E}[\|\hat{\mathbf{H}}_t\|^2 | \mathcal{H}_q = \mathcal{H}_0, \hat{\mathcal{H}}_q = \mathcal{H}_1]$ is the MSE for a false alarm, and $\text{MSE}_{0,1} \triangleq \mathbb{E}[\|\hat{\mathbf{H}}_t - \mathbf{H}_t\|^2 | \mathcal{H}_q = \mathcal{H}_1, \hat{\mathcal{H}}_q = \mathcal{H}_0]$ is the MSE for a miss detection (with $\hat{\mathbf{H}}_t = \mathbf{0}$)². Evaluating these expectations yields $\text{MSE}_{1,1} = \text{MSE}_{1,0} = \sigma_n^2 \frac{N}{P_r}$ and $\text{MSE}_{0,1} = N^2 \sigma_n^2$. Thus, improving P_D not only increases the frequency of valid estimations but also mitigates the impact of miss detections, thereby reducing the overall error and reinforcing how enhanced detection and lowering false alarms directly improves estimation accuracy.

Substituting the PDF in (20) into the GLRT, we obtain,

$$\Lambda(\mathbf{y}_{r,t,l}) = \frac{\sigma_n^{2N} \exp \left(-(\mathbf{y}_{r,t,l} - \hat{\mathbf{H}}_t \mathbf{x}_{t,l})^H \hat{\mathbf{R}}_{1,t}^{-1} (\mathbf{y}_{r,t,l} - \hat{\mathbf{H}}_t \mathbf{x}_{t,l}) \right)_{\mathcal{H}_1}}{\det(\hat{\mathbf{R}}_{1,t}) \exp \left(-\frac{1}{\sigma_n^2} \mathbf{y}_{r,t,l}^H \mathbf{y}_{r,t,l} \right)_{\mathcal{H}_0}} \gtrless \tau_0 \quad (25)$$

where $\hat{\mathbf{R}}_{1,t} = \hat{\mathbf{H}}_t \mathbf{R}_{t,l} \hat{\mathbf{H}}_t^H + \sigma_n^2 \mathbf{I}_N$ and τ_0 is the detection threshold. Taking the logarithm of the likelihood ratio and rearranging terms, the final GLRT form is given by,

$$\dot{\Lambda}(\mathbf{y}_{r,t,l}) = \mathbf{y}_{r,t,l}^H \left(\mathbf{I}_N + \hat{\mathbf{R}}_{1,t}^{-1} \right) \mathbf{y}_{r,t,l} \gtrless \tau_1 \quad (26)$$

where $\tau_1 = \ln \tau_0 + N \ln \sigma_n^2 - \ln \det(\hat{\mathbf{R}}_{1,t})$. Here, the constant terms $N \ln \sigma_n^2$ and $\ln \det(\hat{\mathbf{R}}_{1,t})$ have been absorbed into the threshold. This expression decides the most probable hypothesis, i.e., \mathcal{H}_0 or \mathcal{H}_1 , by incorporating the estimated target response matrix $\hat{\mathbf{H}}_t$ in the covariance matrix $\mathbf{R}_{1,t}$. Since the received signals from different snapshots are conditionally independent, (26) can be updated to adapt to L snapshot scenario by taking the average, i.e., $\bar{\Lambda}_{t,l} = \frac{1}{L} \sum_{l=1}^L \dot{\Lambda}_{t,l} \gtrless \tau_2$, with τ_2 is the detection threshold considering all snapshots and can be designed according to Neyman-Pearson lemma.

B. The KLD of radar system

As the number of snapshots L approaches infinity, the law of large numbers ensures that the estimated target response matrix converges in probability to the true value, i.e., $\hat{\mathbf{H}}_t \xrightarrow{p} \mathbf{H}_t$. This allows us to use \mathbf{H}_t in place of $\hat{\mathbf{H}}_t$ for large L . Under this assumption, we can proceed with a more tractable derivation of the KLD for the radar subsystem.

Using this property, we can now derive the $\text{KLD}_{r,t}^{\mathcal{H}_0 \rightarrow \mathcal{H}_1}$ for the radar subsystem using the probability density functions established in (20), and (6) as follows,

$$\text{KLD}_{r,t}^{\mathcal{H}_0 \rightarrow \mathcal{H}_1} = \frac{1}{\ln 2} \left(\ln(\det(\mathbf{R}_{2,t})) + \text{Tr} \left(\mathbf{R}_{2,t}^{-1} (\sigma_n^2 \mathbf{I}_N) \right) \right. \\ \left. - N (1 + \ln(\sigma_n^2)) \right), \quad (27)$$

where $\mathbf{R}_{2,t} = \frac{1}{L} \sum_{l=1}^L \mathbf{R}_{1,t} = \mathbf{H}_t \frac{1}{L} \sum_{l=1}^L \mathbf{R}_{t,l} \mathbf{H}_t^H + \sigma_n^2 \mathbf{I}_N = \mathbf{H}_t \mathbf{R}_t \mathbf{H}_t^H + \sigma_n^2 \mathbf{I}_N$, and $\det(\cdot)$ is the determinant operation.

² $\text{MSE}_{0,0} \triangleq 0$ is not used because when the target is absent and correctly declared absent, both the true and estimated \mathbf{H}_t are zero, yielding no error.

$\text{KLD}_{r,t} = \frac{1}{2} \left(\text{KLD}_{r,t}^{\mathcal{H}_0 \rightarrow \mathcal{H}_1} + \text{KLD}_{r,t}^{\mathcal{H}_1 \rightarrow \mathcal{H}_0} \right)$, where in this case $\text{KLD}_{r,t}^{\mathcal{H}_0 \rightarrow \mathcal{H}_1} = \text{KLD}_{r,t}^{\mathcal{H}_1 \rightarrow \mathcal{H}_0}$.

V. RADAR WAVEFORM OPTIMISATION

In this section, the radar waveform is optimised while using the ZF beamforming scheme for the communication subsystem. The optimisation problem is,

$$\mathcal{P}_1 : \max_{\dot{\mathbf{W}}_r} \frac{1}{T} \sum_{t=1}^T \text{KLD}_{r,t} | \mathbf{W}_{r,t}, \mathbf{H}_t \quad (28a)$$

$$\text{s.t. } \text{KLD}_{r,t} \geq \underline{A}_t, \forall t \in T, \quad (28b)$$

$$\text{KLD}_{c,k} \geq \underline{B}_k, \forall k \in K, \quad (28c)$$

$$\sum_{t=1}^T \frac{1}{L} \|\mathbf{W}_{r,t}\|_F^2 \leq P_r, \quad (28d)$$

$$P_c = P_T - P_r, \quad (28e)$$

where $\text{KLD}_{r,t} | \mathbf{W}_{r,t}, \mathbf{H}_t$ is defined in (27). After substituting (27) in (28a), can be written as \mathcal{P}_2 that is given on page 7. This optimisation problem focuses on the radar waveform while considering the whole ISAC system performance. The minimum KLD requirements in constraints (28b) and (28c) are carefully chosen to ensure specific performance guarantees in terms of detection probability P_D and BER for the radar and communication subsystems, respectively. The constraint on radar power (28d) is explicit because the radar waveform is our primary optimisation variable. The communication power is implicitly considered through the ZF beamforming scheme and the constraint (28c) on communication performance. Specifically, the communication subsystem utilises its allocated power through the ZF beamforming scheme to distribute power to each UE, with weights predetermined based on the channel state information. To solve the optimisation problem in (29), we utilise the Projected Gradient method with a penalty function [37]. This method is chosen for its suitability to the non-linear, non-convex optimisation problem [38]. This method uses a penalty function for KLD constraints and handles radar power via projection, balancing the solution quality and computational efficiency for real-time ISAC applications. Its scalability makes it suitable for radar waveform optimisation in ISAC. The optimisation variable $\dot{\mathbf{W}}_r \in \mathbb{C}^{N \times L \times T}$ is a three-dimensional tensor, where $\mathbf{w}_{r,t,l}$, $\mathbf{W}_{r,t}$, and $\mathbf{W}_{r,l}$ are all parts of this tensor. We define the objective function $f(\dot{\mathbf{W}}_r)$ and a penalty function $p(\dot{\mathbf{W}}_r)$ to handle the constraints in (28b) and (28c),

$$f(\dot{\mathbf{W}}_r) = \frac{1}{T} \sum_{t=1}^T \text{KLD}_{r,t} | \mathbf{W}_{r,t}, \mathbf{H}_t, \quad (30)$$

$$p(\dot{\mathbf{W}}_r) = \sum_{t=1}^T \left(\max(0, \underline{A}_t - \text{KLD}_{r,t} | \mathbf{W}_{r,t}, \mathbf{H}_t)^2 \right) + \sum_{k=1}^K \left(\max(0, \underline{B}_k - \text{KLD}_{c,k} | \dot{\mathbf{W}}_r)^2 \right). \quad (31)$$

The gradient of the objective function, $\nabla f(\dot{\mathbf{W}}_r) \in \mathbb{C}^{N \times L \times T}$, is a gradient tensor computed element-wise, as detailed in Appendix I.A. The final equation is given by,

$$[\nabla f(\dot{\mathbf{W}}_r)]_{i,l,t} = \frac{2 d_{r,t}^\zeta}{T L \ln 2} \left(\mathbf{H}_t^H (\mathbf{R}_{2,t})^{-1} \mathbf{H}_t \mathbf{W}_{r,t} - \sigma_n^2 (\mathbf{R}_{2,t})^{-2} \mathbf{H}_t \mathbf{W}_{r,t} \right)_i. \quad (32)$$

Algorithm 1 Projected Gradient Method with Penalty for Radar Waveform Optimisation

Require: Initial point $\dot{\mathbf{W}}_r^{(0)}$, constants $\alpha_0, \rho_0, \beta, \gamma, c, P_r, \underline{A}_t, \underline{B}_k$, tolerance ε , and maximum iterations max_iter
Ensure: Optimal solution $\dot{\mathbf{W}}_r^*$

- 1: Initialise $n = 0$
- 2: **while** $n < \text{max_iter}$ **do**
- 3: Compute gradients $\nabla f(\dot{\mathbf{W}}_r^{(n)})$ and $\nabla p(\dot{\mathbf{W}}_r^{(n)})$
- 4: Compute total gradient $\mathbf{G}^{(n)} = \nabla f(\dot{\mathbf{W}}_r^{(n)}) - \rho_n \nabla p(\dot{\mathbf{W}}_r^{(n)})$
- 5: Perform backtracking line search to find α_n
- 6: Update $\dot{\mathbf{W}}_r^{(n+1)} = \mathcal{P}(\dot{\mathbf{W}}_r^{(n)} + \alpha_n \mathbf{G}^{(n)})$
- 7: Compute $f(\dot{\mathbf{W}}_r^{(n+1)})$ and $p(\dot{\mathbf{W}}_r^{(n+1)})$
- 8: Update ρ_{n+1} according to the penalty update rule
- 9: **if** $\|\dot{\mathbf{W}}_r^{(n+1)} - \dot{\mathbf{W}}_r^{(n)}\|_F < \varepsilon$ **then**
- 10: **break**
- 11: **end if**
- 12: $n = n + 1$
- 13: **end while**
- 14: **return** $\dot{\mathbf{W}}_r^* = \dot{\mathbf{W}}_r^{(n)}$

The gradient of the penalty function $\nabla p(\dot{\mathbf{W}}_r) \in \mathbb{C}^{N \times L \times T}$ is also a gradient tensor, computed as,

$$[\nabla p(\dot{\mathbf{W}}_r)]_{i,l,t} = -2(\underline{A}_t - \text{KLD}_{r,t}) [\nabla \text{KLD}_{r,t}]_{i,l} \cdot \mathbb{I}_1 - \sum_{k=1}^K 2(\underline{B}_k - \text{KLD}_{c,k}) [\nabla \text{KLD}_{c,k}]_{i,l,t} \cdot \mathbb{I}_2, \quad (33)$$

where $\mathbb{I}_1 = \mathbb{I}(\text{KLD}_{r,t} < \underline{A}_t)$ and $\mathbb{I}_2 = \mathbb{I}(\text{KLD}_{c,k} < \underline{B}_k)$ with $\mathbb{I}(\cdot)$ represents the indicator function. The gradients of KLD_r and KLD_c with respect to $\mathbf{W}_{r,t}$ and $\dot{\mathbf{W}}_r$, respectively, are provided in Appendix I.A. The final forms are given by,

$$[\nabla \text{KLD}_{r,t} | \mathbf{W}_{r,t}, \mathbf{H}_t]_{i,l} = \frac{2 d_{r,t}^\zeta}{L \ln 2} \left(\mathbf{H}_t^H \mathbf{R}_{2,t}^{-1} \mathbf{H}_t \mathbf{W}_{r,t} - \sigma_n^2 \mathbf{H}_t^H \mathbf{R}_{2,t}^{-2} \mathbf{H}_t \mathbf{W}_{r,t} \right)_i, \quad (34)$$

$$[\nabla \text{KLD}_{c,k} | \dot{\mathbf{W}}_r, \mathbf{H}_t]_{i,l,t} = -\frac{2 d_{c,k}^\zeta \lambda p_k (N-K) \sigma_n^2}{M(M-1) L \sigma_\eta^2 \ln 2} [\dot{\mathbf{W}}_r]_{i,l,t}. \quad (35)$$

The update rule for the projected gradient method with penalty ensures that each iteration moves the solution towards optimality while maintaining feasibility, and can be shown as follows,

$$\dot{\mathbf{W}}_r^{(n+1)} = \mathcal{P} \left(\dot{\mathbf{W}}_r^{(n)} + \alpha_n \mathbf{G}^{(n)} \right), \quad (36)$$

where $\mathbf{G}^{(n)} = \nabla f(\dot{\mathbf{W}}_r^{(n)}) - \rho_n \nabla p(\dot{\mathbf{W}}_r^{(n)})$ is the gradient direction, combining the objective function gradient and the penalty function gradient, ρ_n is the penalty parameter, balancing the objective and constraint satisfaction, α_n is the step size, and \mathcal{P} is the projection onto the feasible set defined by the power constraint, ensuring that the power constraint in (28d) is always satisfied. The projection mechanism is shown as,

$$\mathcal{P}(\dot{\mathbf{W}}_r) = \begin{cases} \dot{\mathbf{W}}_r \sqrt{\frac{P_r L}{\|\dot{\mathbf{W}}_r\|_F^2}}, & \text{if } \frac{1}{L} \|\dot{\mathbf{W}}_r\|_F^2 > P_r \\ \dot{\mathbf{W}}_r, & \text{otherwise} \end{cases} \quad (37)$$

The step size α_n is determined using a backtracking line search to ensure convergence. We find the smallest non-negative integer m such that,

$$\begin{aligned}
\mathcal{P}_2 : \max_{\dot{\mathbf{W}}_r} \frac{1}{T} \sum_{t=1}^T \frac{1}{\ln 2} & \left(\ln \left(\det \left(d_{r,t}^\zeta \mathbf{H}_t \left(\frac{1}{L} \mathbf{W}_{r,t} \mathbf{W}_{r,t}^H + \mathbf{W}_c \mathbf{W}_c^H \right) \mathbf{H}_t^H + \sigma_n^2 \mathbf{I}_N \right) \right) \right. \\
& + \text{Tr} \left(\left(d_{r,t}^\zeta \mathbf{H}_t \left(\frac{1}{L} \mathbf{W}_{r,t} \mathbf{W}_{r,t}^H + \mathbf{W}_c \mathbf{W}_c^H \right) \mathbf{H}_t^H + \sigma_n^2 \mathbf{I}_N \right)^{-1} \sigma_n^2 \right) - N(1 + \ln(\sigma_n^2)) \left. \right) \\
\text{s.t.} \quad & (28b), (28c), (28d), \text{ and } (28e)
\end{aligned} \tag{29}$$

$$\begin{aligned}
f(\dot{\mathbf{W}}_r^{(n+1)}) - \rho_n p(\dot{\mathbf{W}}_r^{(n+1)}) & \geq \\
f(\dot{\mathbf{W}}_r^{(n)}) - \rho_n p(\dot{\mathbf{W}}_r^{(n)}) + c\alpha_n \|\mathbf{G}^{(n)}\|_F^2, & \tag{38}
\end{aligned}$$

where $c \in (0, 1)$. This condition, known as the Armijo condition, ensures a sufficient decrease in the penalised objective function [39]. The step size is set as $\alpha_n = \beta^m \alpha_{n-1}$, with $\beta \in (0, 1)$ as a reduction factor. The penalty parameter ρ_n is updated as follows,

$$\rho_{n+1} = \begin{cases} \gamma \rho_n, & \text{if } p(\dot{\mathbf{W}}_r^{(n+1)}) > 0 \\ \rho_n, & \text{otherwise} \end{cases} \tag{39}$$

where $\gamma > 1$ is a constant factor. This adaptive scheme increases the penalty when constraints are violated and keeps it constant when they are satisfied. The projection operator \mathcal{P} ensures that the power constraint is always satisfied. The backtracking line search procedure is used to determine an appropriate step size α_n at each iteration. This adaptive step size selection helps to ensure a sufficient increase in the objective function while maintaining the stability of the algorithm. The line search condition can be expressed as,

$$\phi(\dot{\mathbf{W}}_r^{(n+1)}) \leq \phi(\dot{\mathbf{W}}_r^{(n)}) + c\alpha_n \langle \nabla \phi(\dot{\mathbf{W}}_r^{(n)}), \dot{\mathbf{W}}_r^{(n+1)} - \dot{\mathbf{W}}_r^{(n)} \rangle, \tag{40}$$

where $\phi(\dot{\mathbf{W}}_r) = f(\dot{\mathbf{W}}_r) - \rho_n p(\dot{\mathbf{W}}_r)$ is the penalised objective function. The penalty parameter ρ_n is updated adaptively based on the constraint violation, allowing the algorithm to balance optimisation and constraint satisfaction. If constraints are consistently violated, the increasing penalty will emphasise constraint adherence.

A. Radar waveform BER-constrained optimisation

We form a baseline radar waveform optimisation by replacing the communication KLD constraint with a per-user instantaneous BER requirement in the problem defined in (29) below.

$$\mathcal{P}_3 : \max_{\dot{\mathbf{W}}_r} \frac{1}{T} \sum_{t=1}^T \text{KLD}_{r,t} | \mathbf{W}_{r,t}, \mathbf{H}_t | \tag{41a}$$

$$\text{s.t. } \text{KLD}_{r,t} \geq \underline{A}_t, \quad \forall t \in T, \tag{41b}$$

$$\text{BER}_k \leq \overline{C}_k \quad \forall k \in K, \tag{41c}$$

$$\sum_{t=1}^T \frac{1}{L} \|\mathbf{W}_{r,t}\|_F^2 \leq P_r, \tag{41d}$$

$$P_c = P_T - P_r, \tag{41e}$$

where the communication subsystem uses the ZF beamforming with precoding matrix \mathbf{W}_c and \overline{C}_k is the upper limit of the BER of the k -th user. As such, it is important to define the BER and the SINR for the communication system. The k -th user SINR is defined as,

$$\text{SINR}_k = \frac{d_{c,k}^{-\zeta} |\mathbf{h}_k^T \mathbf{w}_{c,k}|^2}{\sum_{i=1, i \neq k}^K d_{c,k}^{-\zeta} |\mathbf{h}_k^T \mathbf{w}_{c,i}|^2 + d_{c,k}^{-\zeta} \|\mathbf{h}_k^T \tilde{\mathbf{W}}_r\|^2 + \sigma_n^2}, \tag{42}$$

where $\tilde{\mathbf{W}}_r = \frac{1}{L} \sum_{l=1}^L \mathbf{W}_{r,l}$. For M -ary constellations, the BER of user k is approximated by [40],

$$\text{BER}_k \approx \frac{\lambda_c}{M \log_2 M} Q\left(\sqrt{\beta_c \text{SINR}_k}\right), \tag{43}$$

where λ_c and β_c are constellation-dependent constants (e.g., $\lambda_c = 4, \beta_c = 2$ for QPSK). Unlike the unified closed-form gradients in our KLD-based design, this BER objective depends on the $Q(\cdot)$ function in (43), which introduces additional computational complexity in the optimisation process due to its non-elementary nature and the challenges in evaluating its derivatives efficiently. This distinction illustrates the enhanced analytical tractability of the proposed KLD-based approach. The optimisation problem is non-convex and nonlinear due to the Q -function in (43) and $\text{KLD}_{r,t}$. Using the gradients of $\nabla_{\mathbf{W}_r}$ BER_k derived in Appendix C, and the gradients of the constraints derived previously, we employ the same projected gradient method with penalty as in Algorithm 1, to handle the nonconvexities in (41)

VI. COMMUNICATION OPTIMISATION

The communication subsystem optimisation uses the gradient-assisted IPM [41], in contrast to the projected gradient method with penalty used for radar optimisation, due to the different optimisation variable structures. Radar optimisation involves a three-dimensional tensor $\dot{\mathbf{W}}_r \in \mathbb{C}^{N \times L \times T}$, while communication beamforming optimises a two-dimensional matrix $\mathbf{W}_c \in \mathbb{C}^{N \times K}$. This reduced dimensionality makes IPM particularly suitable, potentially offering faster convergence and more precise solutions. The communication waveform is optimised while using the conventional identity covariance (CIC) matrix design for the radar subsystem, with $\mathbf{R}_w = \mathbf{I}_{N \times N} \quad \forall t \in T$. The optimisation problem can be expressed as follows,

$$\mathcal{P}_4 : \max_{\mathbf{W}_c} \frac{1}{K} \sum_{k=1}^K \text{KLD}_{c,k} | \mathbf{W}_c, \mathbf{h}_k | \tag{44a}$$

$$\text{s.t. } \text{KLD}_{r,t} \geq \underline{A}_t, \quad \forall t \in T, \tag{44b}$$

$$\text{KLD}_{c,k} \geq \underline{B}_k, \quad \forall k \in K, \tag{44c}$$

$$\|\mathbf{W}_c\|_F^2 \leq P_c, \tag{44d}$$

$$P_r = P_T - P_c. \tag{44e}$$

Note, that the radar power is uniformly distributed among potential targets, as the radar covariance matrix ensures omnidirectional beam flow. To solve this optimisation problem, we must derive the gradients of the objective function and the constraints. Let's define the objective function as follows,

$$f(\mathbf{W}_c) = \frac{1}{K} \sum_{k=1}^K \text{KLD}_{c,k} | \mathbf{W}_c, \mathbf{h}_k |. \tag{45}$$

To compute the gradient of the objective function, we need to derive the gradients of each component of \mathbf{W}_c . Let $a_k = d_{c,k}^\zeta |\mathbf{h}_k^T \mathbf{w}_{c,k}|^2$. Using the chain rule and properties of matrix derivatives, the gradients can be expressed as follows,

$$\nabla_{\mathbf{w}_{c,j}} |\mathbf{h}_k^T \mathbf{w}_{c,j}|^2 = 2d_{c,k}^\zeta \mathbf{h}_k \mathbf{h}_k^T \mathbf{w}_{c,j}, \quad \forall j \tag{46}$$

$$\nabla_{\mathbf{w}_{c,j}} \text{KLD}_{c,k} = \begin{cases} C \cdot \frac{2d_{c,k}^\zeta \mathbf{h}_k \mathbf{h}_k^T \mathbf{w}_{c,k}}{b_k}, & \text{if } j = k \\ -C \cdot \frac{2d_{c,k}^\zeta \mathbf{h}_k \mathbf{h}_k^T \mathbf{w}_{c,j} \cdot a_k}{b_k^2}, & \text{if } j \neq k \end{cases} \tag{47}$$

Algorithm 2 Interior Point Method for Communication Optimisation

Require: Initial point $\mathbf{W}_c^{(0)}$, constants μ_0 , γ , P_c , \underline{A}_t , \underline{B}_k , tolerance ϵ , and maximum iterations max_iter
Ensure: Optimal solution \mathbf{W}_c^*

- 1: Initialise $n = 0$, $\mu = \mu_0$
- 2: **while** $n < \text{max_iter}$ **do**
- 3: Compute $f(\mathbf{W}_c^{(n)})$, $\nabla f(\mathbf{W}_c^{(n)})$, $g_i(\mathbf{W}_c^{(n)})$, and $\nabla g_i(\mathbf{W}_c^{(n)})$
- 4: Compute KKT conditions
- 5: **if** KKT conditions satisfied within ϵ **then**
- 6: **break**
- 7: **end if**
- 8: Solve Newton system for search direction $\Delta \mathbf{W}_c$
- 9: Perform line search to find step size α
- 10: Update $\mathbf{W}_c^{(n+1)} = \mathbf{W}_c^{(n)} + \alpha \Delta \mathbf{W}_c$
- 11: Update $\mu = \gamma \mu$
- 12: $n = n + 1$
- 13: **end while**
- 14: **return** $\mathbf{W}_c^* = \mathbf{W}_c^{(n)}$

where $C = \frac{\lambda}{2M(M-1)\ln 2}$, and $b_k = d_{c,k}^\zeta \sum_{i=1, i \neq k}^K \|\mathbf{h}_k^T \mathbf{w}_{c,i}\|^2 + \sigma_\eta^2$. Finally, we can express the gradient of the objective function as,

$$\nabla_{\mathbf{w}_{c,k}} f(\mathbf{W}_c) = \frac{d_{c,k}^\zeta C}{K} \sum_{k=1}^K \left(\frac{2\mathbf{h}_k \mathbf{h}_k^T \mathbf{w}_{c,k}}{b_k} - \sum_{j \neq k} \frac{2\mathbf{h}_k \mathbf{h}_k^T \mathbf{w}_{c,j} \cdot a_k}{b_k^2} \right). \quad (48)$$

Next, we need to consider the constraints of our optimisation problem. The power constraint is given by,

$$g(\mathbf{W}_c) = \|\mathbf{W}_c\|_F^2 - P_c \leq 0. \quad (49)$$

The gradient of this constraint is derived as follows,

$$\nabla_{\mathbf{w}_{c,j}} g(\mathbf{W}_c) = 2\mathbf{w}_{c,j}. \quad (50)$$

The gradient of the radar KLD constraint with respect to \mathbf{W}_c is derived as follows,

$$\nabla_{\mathbf{W}_c} \text{KLD}_{r,t} = \frac{d_{r,t}^\zeta}{\ln 2} \left(\mathbf{R}_{2,t}^{-1} \mathbf{H}_t \mathbf{W}_c \mathbf{H}_t^H \right). \quad (51)$$

Solving the optimisation problem defined in equations (44a)-(44d) uses the IPM, as detailed in **Algorithm 2**. This method efficiently addresses constrained optimisation with key parameters: an initial barrier parameter $\bar{\mu}_0$, a barrier reduction factor $\bar{\gamma}$, and a convergence tolerance ϵ . The algorithm iteratively computes the objective function, constraints, and their gradients, checks the Karush-Kuhn-Tucker (KKT) conditions and updates the solution using a Newton system and line search. The barrier parameter $\bar{\mu}$ is updated as $\bar{\mu} = \bar{\gamma} \bar{\mu}$ in each iteration, gradually enforcing constraints more strictly. This continues until $\|\mathbf{W}_c^{(n+1)} - \mathbf{W}_c^{(n)}\|_F < \epsilon$ or the maximum iterations are reached, yielding the optimal beamforming matrix \mathbf{W}_c^* that maximises the communication KLD while satisfying radar and power constraints.

A. Communication waveform BER-optimisation

We formulate another baseline design that minimises the instantaneous BER with respect to \mathbf{W}_c , while ensuring a minimum

radar KLD per target. The SINR for the k -th user is defined in (42), and the instantaneous BER of user k is approximated by (43). The optimisation problem is,

$$\mathcal{P}_5 : \min_{\mathbf{W}_c} \frac{1}{K} \sum_{k=1}^K \text{BER}_k | \mathbf{W}_c, \mathbf{h}_k \quad (52a)$$

$$\text{s.t. } \text{KLD}_{r,t} \geq \underline{A}_t, \quad \forall t \in T, \quad (52b)$$

$$\text{BER}_k \leq \bar{C}_k, \quad \forall k \in K, \quad (52c)$$

$$\|\mathbf{W}_c\|_F^2 \leq P_c, \quad (52d)$$

$$P_r = P_T - P_c. \quad (52e)$$

where radar subsystem precoder \mathbf{W}_r uses the identity covariance $\mathbf{R}_w = \mathbf{I}_N$. This problem is inherently non-convex and nonlinear due to the Q -function in (43) and $\text{KLD}_{r,t}$ constraint. Using the gradients of $\nabla_{\mathbf{W}_c} \text{BER}_k$ derived in Appendix C, and the constraint gradients derived in (49)-(51), we employ the same gradient-assisted IPM as in Algorithm 2, to handle the nonconvexities in (52), leveraging the reduced dimensionality of $\mathbf{W}_c \in \mathbb{C}^{N \times K}$.

VII. COMPLEXITY ANALYSIS

1) *Projected Gradient Method with Penalty*: The projected gradient method with adaptive penalties for radar waveform optimisation, defined in **Algorithm 1**, has an estimated per-iteration complexity as [38], [39],

$$\mathcal{O}(I \times (E + n^3 + (k+1) \times E + m \times n^2)), \quad (53)$$

where I is the number of iterations, E denotes the cost of evaluating the objective function and its gradients, n represents the number of optimisation variables in the tensor \mathbf{W}_r , m is the number of constraints, and k is the number of backtracking line search iterations per step. The dominant n^3 term arises from matrix operations in the projection step. Although the asymptotic order is the same for both formulations, the BER-based approach generally incurs a higher evaluation cost E due to additional numerical computations in its gradient evaluation.

2) *Gradient-assisted IPM*: For communication waveform optimisation, we utilise a gradient-assisted Interior Point Method as outlined in Algorithm 2. Its per-iteration complexity is [42],

$$\mathcal{O}(I \times (E + n^3 + m \times n^2)), \quad (54)$$

where n denotes the number of optimisation variables in the matrix \mathbf{W}_c . Again, while the dominant n^3 term reflects matrix operations which are common to both methods, the BER-based formulation typically involves a larger constant in E , thereby increasing the overall computational burden.

Overall, while both BER-based and KLD-based waveform optimisations share similar asymptotic complexities dominated by matrix operations, the additional evaluation overhead in BER-based formulations leads to considerably higher practical computational costs.

VIII. NUMERICAL RESULTS

In this section, we present simulation results for our conventional benchmarks and the two previously introduced optimisation techniques. The total transmit power is fixed at $P_T = 1$, and QPSK modulation is used throughout this section. The base station has $N = 20$ antennas, with $L = 100$ snapshots, a maximum of $T = 3$ potential radar targets and $K = 3$ UEs are deployed. A pathloss exponent of $\eta = 3$ is considered to

model large-scale fading. The distances from the BS to the UEs are $d_{c,k} = \{150, 210, 100\} \forall k \leq K$ meters and to the targets are $d_{r,t} = \{100, 115, 95\} \forall t \leq T$ meters. The channel variance is fixed at $\sigma_h^2 = 1$, and the probability of false alarm P_{FA} is set to 10^{-4} . \bar{C}_k is set to 10^{-2} which is approximately equivalent to the KLD_c of 10 bits.

A. Trade-off for the conventional benchmark

The radar subsystem employs a CIC matrix design, with $\mathbf{R}_w = \mathbf{I}_N$, while the communication subsystem utilises the previously introduced ZF. Fig.1 presents the ISAC system per-

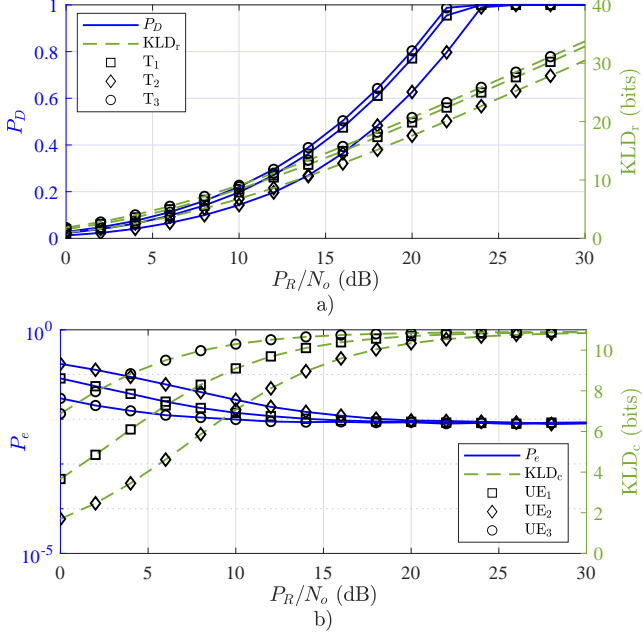


Fig. 1. The ISAC system performance at $P_r = 0.5$. a) Radar subsystem CIC design performance: P_D and KLD_r vs P_R/N_o . b) Communication subsystem ZF precoding performance: BER and KLD_c vs P_R/N_o .

formance, analysing both its radar and communication subsystems at $P_c = 0.5$. The analysis encompasses the radar subsystem's target detection capabilities and the communication subsystem's data transmission quality. Fig.1.a presents the performance of the radar subsystem, illustrated in terms of the KLD_r on the right y -axis and the probability of detection P_D on the left y -axis against P_R/N_o for three potential targets T₁, T₂, and T₃. The curves for all three targets exhibit a consistent upward trend with increasing P_R/N_o , indicating that higher P_R/N_o levels enhance the radar subsystem's capability to distinguish and detect targets. It can be observed from the figure that at $P_R/N_o = 10$ dB, the KLD_r values for T₁, T₂, and T₃ are approximately {8.43, 6.77, 9.1} bits, respectively, while the corresponding detection probabilities P_D reach {0.197, 0.143, 0.221}. By the time P_R/N_o increases to 20 dB, the KLD_r improves to around {19.87, 17.59, 20.71} bits, and P_D increases to {0.771, 0.627, 0.803}. Throughout these P_R/N_o values, T₃ remains the most detectable target, consistently demonstrating the highest KLD_r and P_D , followed by T₁ and then T₂. The consistent rise in both KLD_r and P_D with increasing P_R/N_o demonstrates the strong correlation between the two measures, confirming the validity of utilising KLD_r as a reliable measure of radar performance, as well as a reliable design tool. Higher KLD_r values are directly translated to improved detection probabilities, reinforcing that KLD_r effectively

captures the system's ability to distinguish targets. Fig.1.b shows the performance of the communication subsystem under the ZF precoding scheme, where the KLD on the right y -axis and the BER on the left y -axis are plotted versus P_R/N_o for three single-antenna UEs. As can be observed from the figure, as P_R/N_o increases, the KLD for all UEs rises, reflecting enhanced signal distinguishability. Correspondingly, the BER decreases, indicating better communication quality. Around 10 dB, however, both an upper bound in KLD and an error floor in BER become evident, highlighting the persistent radar interference as the dominant performance limiting factor once IUI has been largely cancelled by ZF at $P_c = 0.5$. Thereby this validates the use of KLD as an effective tool for characterising and designing communication systems since higher KLD values systematically align with lower BER.

B. Radar Waveform KLD-based Optimisation

The radar waveform KLD-based optimisation algorithm is set with a maximum number of iterations of $\text{max_iter} = 1000$, convergence tolerance $\epsilon = 10^{-6}$, initial penalty $\rho_0 = 1$, penalty increase $\gamma = 1.5$, and initial step size $\alpha_0 = 0.1$. The KLD lower bounds \underline{A}_t and \underline{B}_k for all targets and UEs are 10 bits, while the BER upper limit for the BER constrained case \bar{C}_k for all UEs is set to 10^{-2} , the KLD equivalent of around 10 bits for fair comparison.

Fig. 2 illustrates the performance of both subsystems using both KLD-based radar waveform optimisation (K-ROP) and BER-constrained radar waveform optimisation (B-ROP) techniques. In Fig. 2.a, the achievable KLD_r on the right axis and detection probability P_D on the left axis versus P_R/N_o are shown for each target. As can be depicted from the figure, as P_R/N_o increases, both measures improve for all targets, indicating enhanced radar performance. The results in this figure also show a noticeable improvement can be obtained using K-ROP when compared to B-ROP. Moreover, by comparing the results here with the ZF-based design in Fig. 1, it can be noticed that there is a significant gain can be achieved using K-ROP. For example, at $P_R/N_o = 18$ dB, the achievable P_D is {98, 89.2, 99.9}% for T₁, T₂, and T₃ using K-ROP, compared to {61, 48.3, 64.2}% in the non-optimised ZF in Fig. 1, while B-ROP achieves {96.8, 87.5, 98.7}%, demonstrating improved detection capabilities through both optimisation techniques with K-ROP showing a slight improvement in terms of performance. For K-ROP, T₃ consistently achieves the highest KLD_r , followed by T₁ and T₂, reflecting their distances from the BS. At $P_R/N_o = 10$ dB, the $\{KLD_{r,1}, KLD_{r,2}, KLD_{r,3}\}$ values are approximately {11.78, 8.06, 13.38} bits, increasing to {48.06, 39.68, 51.31} bits at $P_R/N_o = 20$ dB. For B-ROP, lower values are achieved, with $\{KLD_{r,1}, KLD_{r,2}, KLD_{r,3}\}$ approximately {10.96, 7.49, 12.44} bits at $P_R/N_o = 10$ dB, increasing to {44.69, 36.91, 47.72} bits at $P_R/N_o = 20$ dB. The rate of KLD_r improvement after 15 dB suggests a near-linear relationship with P_R/N_o for both techniques, indicating consistent performance enhancement in the radar system.

Fig. 2.b illustrates the communication subsystem performance, showing KLD_c on the right axis and BER on the left axis versus P_R/N_o . For K-ROP, UE₃ consistently achieves the highest KLD_c , followed by UE₁ and UE₂. At $P_R/N_o = 10$ dB, the values $\{KLD_{c,1}, KLD_{c,2}, KLD_{c,3}\}$ are approximately {55.14, 20.09, 186.09} for UE₁, UE₂, and UE₃, increasing to

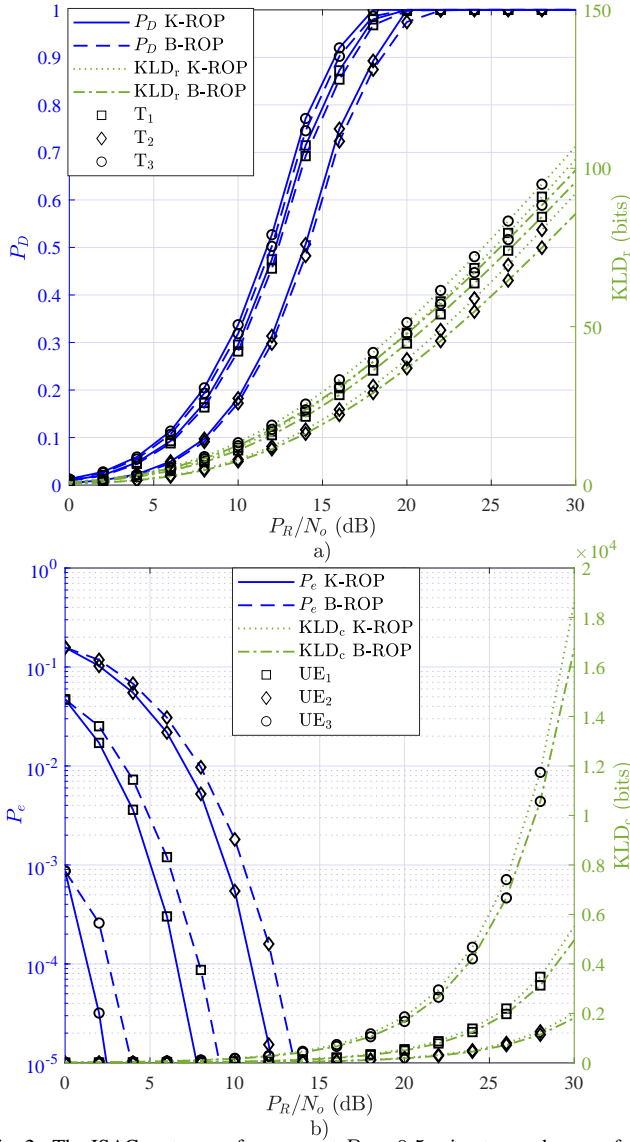


Fig. 2. The ISAC system performance at $P_r = 0.5$ using two radar waveform optimisations: K-ROP and B-ROP. a) Radar subsystem performance: P_D and KLD_r vs P_R/N_o . b) Communication subsystem performance: BER and KLD_c vs P_R/N_o .

$\{551.38, 200.94, 1860.91\}$ at $P_R/N_o = 20$ dB. B-ROP demonstrates similar trends with slightly lower performance, achieving $\{KLD_{c,1}, KLD_{c,2}, KLD_{c,3}\}$ values of $\{49.62, 18.07, 167.48\}$ bits at $P_R/N_o = 10$ dB and $\{496.2, 180.84, 1674.79\}$ bits at $P_R/N_o = 20$ dB. The sharp increase in KLD_c beyond 8 dB for both techniques suggests they have reached their optimisation feasibility points, significantly enhancing the communication performance as the radar interference is effectively reduced. The BER performance shows that K-ROP achieves P_e below 10^{-5} by 13 dB, while B-ROP reaches this threshold at 14 dB, both significantly outperforming the non-optimised ZF case where P_e saturates at 8×10^{-3} after 15 dB as depicted from Fig. 1. These results highlight the intricate relationship between radar detection capabilities and communication system performance, with K-ROP demonstrating slightly superior performance over B-ROP while maintaining similar performance trends.

C. Communication Waveform KLD-based Optimisation

The communication waveform KLD-based optimisation algorithm is configured similarly to the radar algorithm, with a

maximum iteration limit of $\text{max_iter} = 1000$ and a convergence tolerance of $\epsilon = 10^{-6}$. The barrier parameter is initialised at $\tilde{\mu}_0 = 1$ and the barrier reduction factor at $\tilde{\gamma} = 0.1$. The KLD lower bounds for all targets and UEs, \underline{A}_t and \underline{B}_k , are set to 10 bits, while the BER upper limit for the BER constrained case \overline{C}_k for all UEs is set to 10^{-2} , the KLD equivalent of around 10 bits for fair comparison.

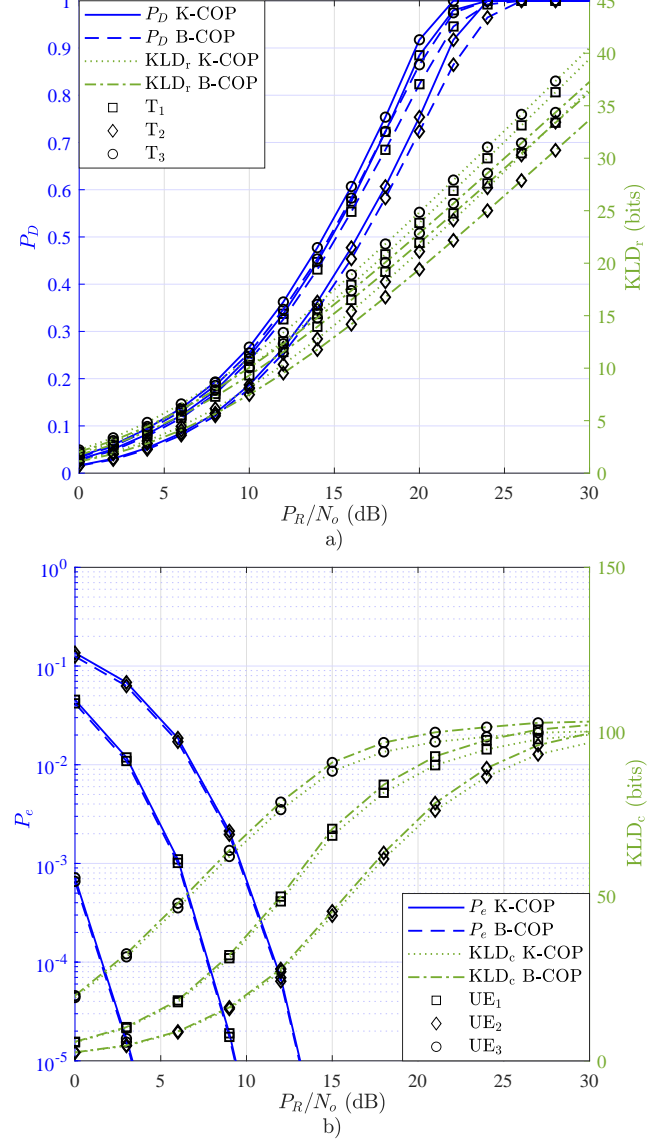


Fig. 3. The ISAC system performance at $P_r = 0.5$ using two communication waveform optimisations: K-COP and B-COP. a) Radar subsystem performance: P_D and KLD_r vs P_R/N_o . b) Communication subsystem performance: BER and KLD_c vs P_R/N_o .

Fig. 3 illustrates the performance of both subsystems using both KLD-based communication waveform optimisation (K-COP) and BER-based communication waveform optimisation (B-COP) techniques. In Fig. 3.a, the achievable KLD_r (right axis) and detection probability P_D (left axis) versus P_R/N_o are shown for each target. For K-COP, as P_R/N_o increases, KLD_r improves across all targets, with target T₃ consistently achieving the highest KLD_r , followed by T₂ and T₁. At $P_R/N_o = 10$ dB, the $\{KLD_{r,1}, KLD_{r,2}, KLD_{r,3}\}$ values are approximately $\{10.12, 8.13, 10.91\}$ bits, increasing to $\{23.84, 21.1, 24.85\}$ bits at $P_R/N_o = 20$ dB. B-COP shows slightly lower KLD_r performance, with values $\{9.31, 7.48, 10.04\}$ bits at $P_R/N_o = 10$ dB.

dB, rising to $\{21.93, 19.42, 22.86\}$ bits at $P_R/N_o = 20$ dB. The linear improvement in KLD_r beyond 15 dB for both techniques indicates stable radar performance despite the suboptimal waveform. At $P_R/N_o = 18$ dB, the P_D values for K-COP are $\{72.2, 60.7, 75.4\}\%$ for T_1, T_2 , and T_3 , while B-COP achieves $\{68.5, 58.2, 72.3\}\%$, compared to $\{61, 48.3, 64.2\}\%$ for the non-optimised ZF shown in Fig. 1. Both techniques demonstrate improved detection capabilities over non-optimisation but remain below the radar waveform optimisation performance achieved using K-ROP in Fig. 2 which is $\{98, 89.2, 99.9\}\%$.

Fig. 3.b illustrates the communication subsystem performance, showing KLD_c (right axis) and BER (left axis) versus P_R/N_o . For K-COP, UE_3 achieves the highest KLD_c , followed by UE_2 and UE_1 . For instance, at $P_R/N_o = 10$ dB, the $\{KLD_{c,1}, KLD_{c,2}, KLD_{c,3}\}$ values are approximately $\{36.94, 19.55, 66.52\}$ bits, rising to $\{87.06, 71.15, 95.94\}$ bits at $P_R/N_o = 20$ dB. Interestingly, B-COP demonstrates marginally better communication performance with $\{KLD_{c,1}, KLD_{c,2}, KLD_{c,3}\}$ values of $\{38.05, 20.133, 68.86\}$ bits at $P_R/N_o = 10$ dB and $\{89.67, 73.29, 98.81\}$ bits at $P_R/N_o = 20$ dB. The BER performance reflects this trend, with B-COP achieving slightly better performance than K-COP. In the non-optimised ZF scenario, P_e saturates at 8×10^{-3} after 15 dB (Fig. 1), while with K-COP optimisation, P_e drops below 10^{-5} by 14 dB across all UEs. B-COP achieves this threshold marginally earlier at 13.5 dB. Both optimisation techniques provide significant performance gains over the non-optimised ZF scenario, though these gains are less pronounced than those achieved through radar waveform optimisation in Sec. VIII-B due to radar interference. The communication performance shows less sharp improvement at higher P_R/N_o due to the need to balance radar subsystem performance with communication enhancements.

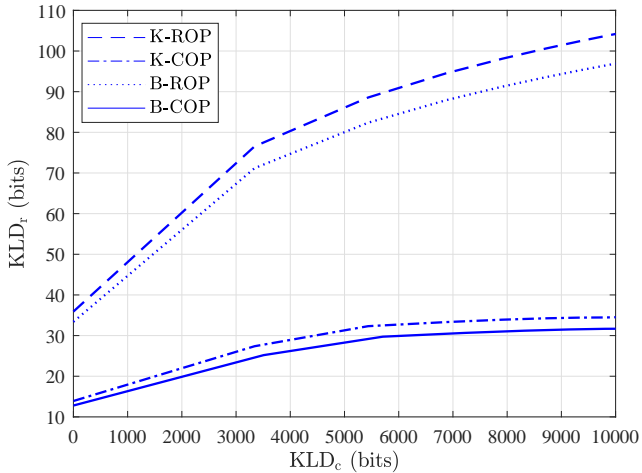


Fig. 4. Trade-off between KLD_c and KLD_r for different optimisation techniques.

Fig. 4 presents the trade-off between the communication and radar subsystems by plotting KLD_c versus KLD_r for various optimisation techniques at $P_R/N_o = 30$ dB, where the power allocation ratio is varied over $0 < P_r < 1$. The K-ROP demonstrates superior performance, achieving higher KLD_r values of up to 105 bits while maintaining significant KLD_c performance. The B-ROP shows slightly lower performance but follows a similar trend, reaching approximately 95 bits in KLD_r . The communication-centric techniques, K-COP and B-COP, while

achieving high KLD_c values of up to 10,000 bits, show more modest radar performance with KLD_r saturating around 35 bits. The curves demonstrate that utilising the improved system model with radar waveform optimisation techniques provide better balanced performance across both subsystems, while communication waveform approaches favour communication performance at the cost of reduced radar capability. This trade-off analysis provides valuable insights for system designers in choosing the appropriate optimisation strategy based on specific application requirements. Fig. 5 presents the average CPU time versus an-

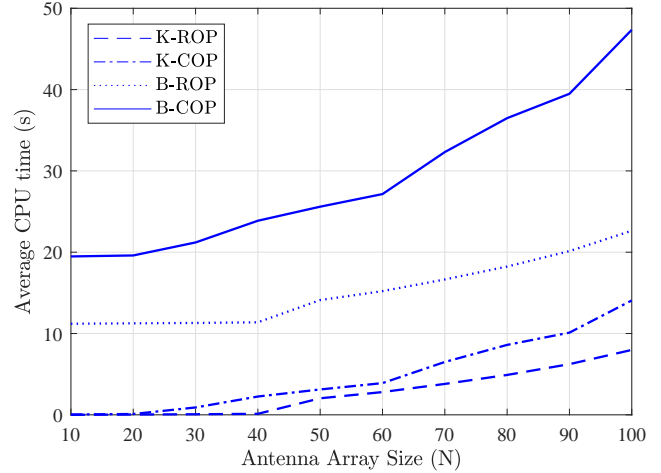


Fig. 5. Average CPU time (seconds) versus antenna array size N for different optimisation techniques.

tenna array size N comparing the four optimisation techniques. The K-ROP demonstrates superior computational efficiency, with CPU time increasing gradually from 0.001 seconds at $N = 10$ to 7.98 seconds at $N = 100$. The K-COP shows moderate computational requirements, ranging from 0.04 to 14.07 seconds across the same range of N . The BER techniques exhibit higher computational demands, with B-ROP requiring between 11.20 and 22.64 seconds, while B-COP shows the highest computational complexity, increasing from 19.48 to 47.35 seconds as N grows from 10 to 100. The substantial difference in computational requirements between KLD-based and BER approaches is evident throughout different array sizes. For instance, at $N = 50$, K-ROP requires only 2.80 seconds compared to 15.21 seconds for B-ROP, while K-COP needs 3.90 seconds versus 27.15 seconds for B-COP. This marked computational advantage of KLD-based optimisation makes it particularly attractive for practical ISAC implementations across all array sizes, with the efficiency gap becoming more pronounced as the number of antennas increases.

Fig. 6 presents the average MSE of the estimated target response matrix $\hat{\mathbf{H}}_t$ averaged for all targets versus P_R/N_o for the four optimisation techniques. At low P_R/N_o values (0-10 dB), all techniques exhibit similar performance with MSE around 0.5, indicating limited estimation accuracy in the low SNR regime. As P_R/N_o increases beyond 10 dB, the techniques begin to show distinct performance characteristics. K-ROP and B-ROP demonstrate better estimation performance, achieving high decaying rate in MSE, particularly in the 15-20 dB range. The K-COP and B-COP, while showing consistent improvement with increasing P_R/N_o , exhibit slightly slower convergence to zero MSE. All techniques eventually achieve negligible MSE at high SNR but at different SNR values. Notably, this MSE performance strongly

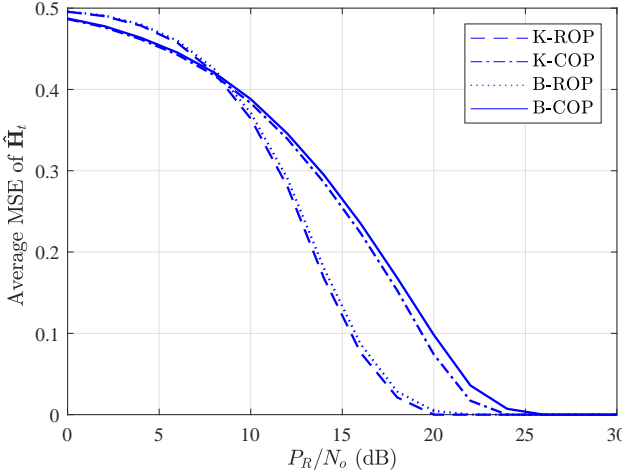


Fig. 6. Average MSE of the target response matrix versus P_R/N_o for different optimisation techniques.

correlates with the detection capabilities shown in Fig. 3.a and 2.a, where techniques achieving higher detection probabilities demonstrate lower estimation errors. This inverse relationship arises as reliable target detection ensures accurate response matrix estimation under \mathcal{H}_1 , while missed detections or false alarms lead to erroneous zero or noise-based estimates, respectively.

IX. CONCLUSION

This paper has proposed and validated a novel KLD-based framework for optimising ISAC systems. The two considered optimisation techniques, namely, KLD-based radar waveform optimisation and KLD-based communication precoding optimisation, were thoroughly evaluated against BER-based baseline optimisation techniques. The KLD-based approaches achieved comparable performance to BER-based methods while offering significantly reduced computational complexity. Radar waveform KLD-based optimisation yielded substantial enhancements in both target detection and communication performance while maintaining efficient computational requirements. Communication KLD-based precoding optimisation, while primarily benefiting the communication subsystem, also showed modest improvements in radar performance, particularly at lower SNRs. Both techniques exhibited robust performance across varying SNR levels, with superior computational efficiency compared to their BER-based counterparts. Moreover, trade-off analysis revealed that incorporating the communication signal in radar detection significantly enhances the overall ISAC system performance. These findings provide valuable insights for designing and optimising shared deployment ISAC systems, offering a promising approach to balance sensing and communication requirements in future wireless networks. The proposed framework provides the means for a holistic ISAC design, paving the way for more efficient and versatile wireless communications and sensing technologies. Future work will explore the synergistic interplay between KLD and machine learning in ISAC, and further practical interference exploitation strategies that address signalling overhead constraints, further enhancing system performance. In addition, to exploring fully combined waveform optimisation in a single problem.

APPENDIX

This appendix provides detailed derivations for the gradients used in our optimisation problem.

A. Gradients for Radar-Waveform Optimisation

The objective function $f(\dot{\mathbf{W}}_r)$ is given in (30), where the $\text{KLD}_{r,t}$ is defined in (27). Therefore, to derive $\nabla f(\dot{\mathbf{W}}_r)$, we first compute $\partial \text{KLD}_{r,t} / \partial \mathbf{W}_{r,t}$. Using the matrix identity $\frac{\partial \ln(\det(\mathbf{X}))}{\partial \mathbf{X}} = (\mathbf{X}^{-1})^T$, and derivative $\frac{\partial \text{Tr}(\mathbf{X}^{-1} \mathbf{A})}{\partial \mathbf{X}} = -(\mathbf{X}^{-1})^T \mathbf{A}^T (\mathbf{X}^{-1})^T$ we obtain,

$$\frac{\partial \ln(\det(\mathbf{R}_{2,t}))}{\partial \mathbf{R}_{2,t}} = \mathbf{R}_{2,t}^{-1}, \quad \frac{\partial \text{Tr}(\mathbf{R}_{2,t}^{-1} \sigma_n^2)}{\partial \mathbf{R}_{2,t}} = -\sigma_n^2 \mathbf{R}_{2,t}^{-2}. \quad (55)$$

Applying the chain rule to (27), and substituting (55) we get,

$$\frac{\partial \text{KLD}_{r,t}}{\partial \mathbf{W}_{r,t}} = \frac{1}{\ln 2} (\mathbf{R}_{2,t}^{-1} - \sigma_n^2 \mathbf{R}_{2,t}^{-2}) \cdot \frac{\partial \mathbf{R}_{2,t}}{\partial \mathbf{W}_{r,t}}, \quad (56)$$

where $\frac{\partial \mathbf{R}_{2,t}}{\partial \mathbf{W}_{r,t}} = \frac{d_{r,t}^\zeta}{L \ln 2} \mathbf{H}_t^H \mathbf{H}_t \mathbf{W}_{r,t}$. Substituting this into (56) and simplifying, we obtain,

$$\frac{\partial \text{KLD}_{r,t}}{\partial \mathbf{W}_{r,t}} = \frac{d_{r,t}^\zeta}{L \ln 2} (\mathbf{H}_t^H \mathbf{R}_{2,t}^{-1} \mathbf{H}_t \mathbf{W}_{r,t} - \sigma_n^2 \mathbf{H}_t^H \mathbf{R}_{2,t}^{-2} \mathbf{H}_t \mathbf{W}_{r,t}). \quad (57)$$

Finally, the gradient of f with respect to $\mathbf{W}_{r,t}$, derived from (30) and (57), is,

$$[\nabla f(\dot{\mathbf{W}}_r)]_{i,l,t} = \frac{2d_{r,t}^\zeta}{TL \ln 2} (\mathbf{H}_t^H \mathbf{R}_{2,t}^{-1} \mathbf{H}_t \mathbf{W}_{r,t} - \sigma_n^2 \mathbf{R}_{2,t}^{-2} \mathbf{H}_t \mathbf{W}_{r,t})_i. \quad (58)$$

For $\text{KLD}_{c,k}$ gradient calculations, we consider how changes in \mathbf{W}_r affect σ_η^2 , where it is defined as follows,

$$\sigma_\eta^2 = d_{c,k}^\zeta \sigma_h^2 \text{Tr}\left(\frac{1}{L} \sum_{l=1}^L \mathbf{W}_{r,l} \mathbf{W}_{r,l}^H\right) + \sigma_n^2 \quad (59)$$

The derivative of σ_η^2 with respect to $\mathbf{W}_{r,l}$ is,

$$\frac{\partial \sigma_\eta^2}{\partial \mathbf{W}_{r,l}} = \frac{2 d_{c,k}^\zeta \sigma_h^2}{L} \mathbf{W}_{r,l}. \quad (60)$$

Computing $\partial \text{KLD}_{c,k} / \partial \sigma_\eta^2$,

$$\frac{\partial \text{KLD}_{c,k}}{\partial \sigma_\eta^2} = -\frac{\lambda d_{c,k}^\zeta p_k (N - K)}{M(M - 1) \sigma_\eta^2 \ln 2}. \quad (61)$$

Utilising the chain rule and (60), (61), we obtain,

$$\frac{\partial \text{KLD}_{c,k}}{\partial \mathbf{W}_{r,l}} = -\frac{2\lambda d_{c,k}^\zeta p_k (N - K) \sigma_h^2}{M(M - 1) L \sigma_\eta^2 \ln 2} \mathbf{W}_{r,l}. \quad (62)$$

Therefore, the gradient of $\text{KLD}_{c,k}$ with respect to $\dot{\mathbf{W}}_r$ is,

$$[\nabla \text{KLD}_{c,k}]_{i,l,t} = -\frac{2\lambda d_{c,k}^\zeta p_k (N - K) \sigma_h^2}{M(M - 1) L \sigma_\eta^2 \ln 2} [\dot{\mathbf{W}}_r]_{i,l,t}. \quad (63)$$

Equations (58) and (63) provide the mathematical foundation for the gradients used in our optimisation algorithm.

B. Gradient of BER w.r.t. \mathbf{W}_r

Using the chain rule, the gradient of BER_k w.r.t. \mathbf{W}_r is,

$$\nabla_{\mathbf{W}_r} \text{BER}_k = \frac{\partial \text{BER}_k}{\partial \text{SINR}_k} \cdot \nabla_{\mathbf{W}_r} \text{SINR}_k, \quad (64)$$

where the partial derivative is,

$$\frac{\partial \text{BER}_k}{\partial \text{SINR}_k} = -\frac{\lambda_c \sqrt{\beta_c}}{2M \log_2 M \sqrt{2\pi \text{SINR}_k}} e^{-\beta_c \text{SINR}_k / 2}, \quad (65)$$

and $\nabla_{\mathbf{W}_r} \text{SINR}_k$ is derived from (42) as follows,

$$\nabla_{\mathbf{W}_r} \text{SINR}_k = -\frac{d_{c,k}^{-2\zeta} |\mathbf{h}_k^T \mathbf{w}_{c,k}|^2}{\mathcal{D}^2} \cdot \frac{2}{L} \mathbf{h}_k^* \mathbf{h}_k^T \tilde{\mathbf{W}}_r. \quad (66)$$

Substituting (66) and (65) in (64), we get the gradient $\nabla_{\mathbf{W}_r} \text{BER}_k$.

C. Gradients of BER w.r.t \mathbf{W}_c

Using the chain rule, the gradient of BER_k w.r.t. \mathbf{W}_c is:

$$\nabla_{\mathbf{W}_c} \text{BER}_k = \frac{\partial \text{BER}_k}{\partial \text{SINR}_k} \cdot \nabla_{\mathbf{W}_c} \text{SINR}_k, \quad (67)$$

where the partial derivative is defined in (65), and $\nabla_{\mathbf{W}_c} \text{SINR}_k$ is derived from (42). Let $\mathcal{D} = d_{c,k}^{-\zeta} \sum_{i \neq k} |\mathbf{h}_k^T \mathbf{w}_{c,i}|^2 + d_{c,k}^{-\zeta} \|\mathbf{h}_k^T \mathbf{W}_r\|^2 + \sigma_n^2$. Then,

$$\begin{aligned} \nabla_{\mathbf{W}_c} \text{SINR}_k &= \frac{2d_{c,k}^{-\zeta}}{\mathcal{D}} \mathbf{h}_k \mathbf{h}_k^T \mathbf{w}_{c,k} \mathbf{e}_k^T \\ &\quad - \frac{2d_{c,k}^{-2\zeta}}{\mathcal{D}^2} \|\mathbf{h}_k^T \mathbf{w}_{c,k}\|^2 \mathbf{h}_k \mathbf{h}_k^T \mathbf{W}_c (\mathbf{I} - \mathbf{e}_k \mathbf{e}_k^T), \end{aligned} \quad (68)$$

where \mathbf{e}_k k -th standard basis vector. Substituting (65) and (68) into (67), we get the gradient $\nabla_{\mathbf{W}_c} \text{BER}_k$.

REFERENCES

- [1] K. Zheng *et al.*, “Reliable and efficient autonomous driving: the need for heterogeneous vehicular networks,” *IEEE Commun. Mag.*, vol. 53, no. 12, pp. 72–79, 2015.
- [2] D. C. Nguyen *et al.*, “6G Internet of Things: A Comprehensive Survey,” *IEEE Internet Things J.*, vol. 9, no. 1, pp. 359–383, 2022.
- [3] P. Porambage *et al.*, “The Roadmap to 6G Security and Privacy,” *IEEE Open J. Commun. Soc.*, vol. 2, pp. 1094–1122, 2021.
- [4] M. Alsabah *et al.*, “6G Wireless Communications Networks: A Comprehensive Survey,” *IEEE Access*, vol. 9, pp. 148 191–148 243, 2021.
- [5] ERICSSON, “Joint communication and sensing in 6G networks,” *Technical Report, Oct. 2021*. [Online]. Available: <https://tinyurl.com/w5t7dwd>
- [6] N. Rajatheva *et al.*, “White Paper on Broadband Connectivity in 6G,” *arXiv preprint arXiv:2004.14247*, 2020. [Online]. Available: <https://doi.org/10.48550/arXiv.2004.14247>
- [7] M. M. Azari *et al.*, “Evolution of Non-Terrestrial Networks From 5G to 6G: A Survey,” *IEEE Commun. Surv. Tutor.*, vol. 24, no. 4, pp. 2633–2672, 2022.
- [8] A. Liu *et al.*, “A Survey on Fundamental Limits of Integrated Sensing and Communication,” *IEEE Commun. Surveys Tuts.*, vol. 24, no. 2, pp. 994–1034, 2022.
- [9] F. Liu, C. Masouros, A. Li, and T. Ratnarajah, “Robust MIMO Beamforming for Cellular and Radar Coexistence,” *IEEE Wireless Commun. Lett.*, vol. 6, no. 3, pp. 374–377, 2017.
- [10] F. Liu *et al.*, “Toward Dual-functional Radar-Communication Systems: Optimal Waveform Design,” *IEEE Trans. Signal Process.*, vol. 66, no. 16, pp. 4264–4279, 2018.
- [11] M. Temiz, E. Alsusa, and M. W. Baidas, “A Dual-Functional Massive MIMO OFDM Communication and Radar Transmitter Architecture,” *IEEE Trans. Veh. Technol.*, vol. 69, no. 12, pp. 14 974–14 988, 2020.
- [12] —, “Optimized Precoders for Massive MIMO OFDM Dual Radar-Communication Systems,” *IEEE Trans. Commun.*, vol. 69, no. 7, pp. 4781–4794, 2021.
- [13] J. A. Zhang *et al.*, “An Overview of Signal Processing Techniques for Joint Communication and Radar Sensing,” *IEEE J. Sel. Topics Signal Process.*, vol. 15, no. 6, pp. 1295–1315, 2021.
- [14] F. Liu *et al.*, “MU-MIMO Communications With MIMO Radar: From Co-Existence to Joint Transmission,” *IEEE Trans. Wireless Commun.*, vol. 17, no. 4, pp. 2755–2770, 2018.
- [15] C. Xu, B. Clerckx, and J. Zhang, “Multi-Antenna Joint Radar and Communications: Precoder Optimization and Weighted Sum-Rate vs Probing Power Tradeoff,” *IEEE Access*, vol. 8, pp. 173 974–173 982, 2020.
- [16] N. Fatema *et al.*, “Massive MIMO Linear Precoding: A Survey,” *IEEE Syst. J.*, vol. 12, pp. 3920–3931, 2018.
- [17] C. Ouyang, Y. Liu, and H. Yang, “Performance of Downlink and Uplink Integrated Sensing and Communications (ISAC) Systems,” *IEEE Wireless Communications Letters*, vol. 11, no. 9, pp. 1850–1854, 2022.
- [18] B. Tang, M. M. Naghsh, and J. Tang, “Relative Entropy-Based Waveform Design for MIMO Radar Detection in the Presence of Clutter and Interference,” *IEEE Trans. Signal Process.*, vol. 63, no. 14, pp. 3783–3796, 2015.
- [19] J. Tang, N. Li, Y. Wu, and Y. Peng, “On Detection Performance of MIMO Radar: A Relative Entropy-Based Study,” *IEEE Signal Process. Lett.*, vol. 16, no. 3, pp. 184–187, 2009.
- [20] Y. Kloob, M. Al-Jarrah, E. Alsusa, and C. Masouros, “Trade-Off Performance Analysis of Radcom Using the Relative Entropy,” in *Proc. IEEE Symp. Comput. Commun. (ISCC) 2024*, pp. 1–6, 2024.
- [21] M. Al-Jarrah, E. Alsusa, and C. Masouros, “A Unified Performance Framework for Integrated Sensing-Communications based on KL-Divergence,” *IEEE Trans. Wireless Commun.*, pp. 1–1, 2023.
- [22] —, “Kullback-Leibler Divergence Analysis for Integrated Radar and Communications (RadCom),” in *2023 IEEE Wireless Commun. Netw. Conf. (WCNC)*, 2023, pp. 1–6.
- [23] Y. Kloob, M. Al-Jarrah, E. Alsusa, and C. Masouros, “Novel KLD-based Resource Allocation for Integrated Sensing and Communication,” *IEEE Trans. Signal Process.*, vol. 72, pp. 2292–2307, 2024.
- [24] Z. Fei *et al.*, “Revealing the trade-Off in ISAC systems: The KL divergence perspective,” *IEEE Wireless Commun. Lett.*, pp. 1–1, 2024.
- [25] F. Liu *et al.*, “Cramér-Rao Bound Optimization for Joint Radar-Communication Beamforming,” *IEEE Trans. Signal Process.*, vol. 70, pp. 240–253, 2022.
- [26] X. Wang, Z. Fei, J. A. Zhang, and J. Xu, “Partially-Connected Hybrid Beamforming Design for Integrated Sensing and Communication Systems,” *IEEE Trans. Commun.*, vol. 70, no. 10, pp. 6648–6660, 2022.
- [27] Z. Liao and F. Liu, “Symbol-Level Precoding for Integrated Sensing and Communications: A Faster-Than-Nyquist Approach,” *IEEE Communications Letters*, vol. 27, no. 12, pp. 3210–3214, 2023.
- [28] A. Hassanien, M. G. Amin, Y. D. Zhang, and F. Ahmad, “Signaling strategies for dual-function radar communications: an overview,” *IEEE Aerosp. Electron. Syst. Mag.*, vol. 31, no. 10, pp. 36–45, 2016.
- [29] P. Kumari, J. Choi, N. González-Prelcic, and R. W. Heath, “IEEE 802.11ad-Based Radar: An Approach to Joint Vehicular Communication-Radar System,” *IEEE Trans. Veh. Technol.*, vol. 67, no. 4, pp. 3012–3027, 2018.
- [30] H. Xu, R. S. Blum, J. Wang, and J. Yuan, “Colocated MIMO radar waveform design for transmit beampattern formation,” *IEEE Trans. Aerosp. Electron. Syst.*, vol. 51, no. 2, pp. 1558–1568, 2015.
- [31] A. Hassanien and S. A. Vorobyov, “Phased-MIMO Radar: A Tradeoff Between Phased-Array and MIMO Radars,” *IEEE Trans. Signal Process.*, vol. 58, no. 6, pp. 3137–3151, 2010.
- [32] H. Zhang, B. Zong, and J. Xie, “Power and Bandwidth Allocation for Multi-Target Tracking in Collocated MIMO Radar,” *IEEE Trans. Veh. Technol.*, vol. 69, no. 9, pp. 9795–9806, 2020.
- [33] H. Zhang *et al.*, “Antenna Selection for Target Tracking in Collocated MIMO Radar,” *IEEE Trans. Aerosp. Electron. Syst.*, vol. 57, no. 1, pp. 423–436, 2021.
- [34] W. Yi, T. Zhou, Y. Ai, and R. S. Blum, “Suboptimal Low Complexity Joint Multi-Target Detection and Localization for Non-Coherent MIMO Radar With Widely Separated Antennas,” *IEEE Trans. Signal Process.*, vol. 68, pp. 901–916, 2020.
- [35] E. Fishler *et al.*, “Spatial Diversity in Radars—Models and Detection Performance,” *IEEE Trans. Signal Process.*, vol. 54, no. 3, pp. 823–838, 2006.
- [36] A. M. Haimovich, R. S. Blum, and L. J. Cimini, “MIMO Radar with Widely Separated Antennas,” *IEEE Signal Process. Mag.*, vol. 25, no. 1, pp. 116–129, 2008.
- [37] J. Nocedal and S. J. Wright, *Numerical Optimization*, 2nd ed. Springer, 2006.
- [38] D. P. Bertsekas, *Nonlinear Programming*, 2nd ed. Athena Scientific, 1999.
- [39] L. Armijo, “Minimization of functions having Lipschitz continuous first partial derivatives,” *Pacific Journal of Mathematics*, vol. 16, no. 1, pp. 1–3, 1966.
- [40] J. Proakis and M. Salehi, *Digital Communications*, ser. McGraw-Hill International Edition. McGraw-Hill, 2008. [Online]. Available: <https://books.google.co.uk/books?id=ksh0GgAACAAJ>
- [41] A. Forsgren, P. E. Gill, and M. H. Wright, “Interior Methods for Nonlinear Optimization,” *SIAM Review*, vol. 44, no. 4, pp. 525–597, 2002. [Online]. Available: <https://doi.org/10.1137/S0036144502414942>
- [42] J. Nocedal and S. J. Wright, *Interior-Point Methods for Linear Programming*, 2nd ed. Springer, 2006, pp. 407–436.